


# Immunoassay-Amplified Responses Using a Functionalized MoS<sub>2</sub>-Based SPR Biosensor to Detect PAPP-A2 in Maternal Serum Samples to Screen for Fetal Down's Syndrome

This article was published in the following Dove Press journal:  
*International Journal of Nanomedicine*


Nan-Fu Chiu <sup>1,2</sup>

Ming-Jung Tai<sup>1</sup>

Devi Taufiq Nurrohman <sup>1,3</sup>

Ting-Li Lin<sup>1</sup>

Ying-Hao Wang<sup>1</sup>

Chen-Yu Chen <sup>4,5</sup>

<sup>1</sup>Laboratory of Nano-Photonics and Biosensors, Institute of Electro-Optical Engineering, National Taiwan Normal University, Taipei City, Taiwan;

<sup>2</sup>Department of Life Science, National Taiwan Normal University, Taipei City, Taiwan; <sup>3</sup>Department of Electronics Engineering, State Polytechnic of Cilacap, Cilacap, Indonesia; <sup>4</sup>Department of Obstetrics and Gynecology, Mackay Memorial Hospital, Taipei City, Taiwan;

<sup>5</sup>Department of Medicine, Mackay Medical College, Taipei City, Taiwan

**Background:** Due to educational, social and economic reasons, more and more women are delaying childbirth. However, advanced maternal age is associated with several adverse pregnancy outcomes, and in particular a high risk of Down's syndrome (DS). Hence, it is increasingly important to be able to detect fetal Down's syndrome (FDS).

**Methods:** We developed an effective, highly sensitive, surface plasmon resonance (SPR) biosensor with biochemically amplified responses using carboxyl-molybdenum disulfide (MoS<sub>2</sub>) film. The use of carboxylic acid as a surface modifier of MoS<sub>2</sub> promoted dispersion and formed specific three-dimensional coordination sites. The carboxylic acid immobilized unmodified antibodies in a way that enhanced the bioaffinity of MoS<sub>2</sub> and preserved biorecognition properties of the SPR sensor surface. Complete antigen pregnancy-associated plasma protein-A2 (PAPP-A2) conjugated with the carboxyl-MoS<sub>2</sub>-modified gold chip to amplify the signal and improve detection sensitivity. This heterostructure interface had a high work function, and thus improved the efficiency of the electric field energy of the surface plasmon. These results provide evidence that the interface electric field improved performance of the SPR biosensor.

**Results:** The carboxyl-MoS<sub>2</sub>-based SPR biosensor was used successfully to evaluate PAPP-A2 level for fetal Down's syndrome screening in maternal serum samples. The detection limit was 0.05 pg/mL, and the linear working range was 0.1 to 1100 pg/mL. The women with an SPR angle >46.57 m° were more closely associated with fetal Down's syndrome. Once optimized for serum Down's syndrome screening, an average recovery of 95.2% and relative standard deviation of 8.5% were obtained. Our findings suggest that carboxyl-MoS<sub>2</sub>-based SPR technology may have advantages over conventional ELISA in certain situations.

**Conclusion:** Carboxyl-MoS<sub>2</sub>-based SPR biosensors can be used as a new diagnostic technology to respond to the increasing need for fetal Down's syndrome screening in maternal serum samples. Our results demonstrated that the carboxyl-MoS<sub>2</sub>-based SPR biosensor was capable of determining PAPP-A2 levels with acceptable accuracy and recovery. We hope that this technology will be investigated in diverse clinical trials and in real case applications for screening and early diagnosis in the future.

**Keywords:** carboxyl-functionalized molybdenum disulfide, carboxyl-MoS<sub>2</sub>, surface plasmon resonance, SPR, pregnancy-associated plasma protein A2, PAPP-A2, Down's syndrome, DS, fetal Down's syndrome, FDS

Correspondence: Nan-Fu Chiu  
Laboratory of Nano-Photonics and Biosensors, Institute of Electro-Optical Engineering, National Taiwan Normal University, No. 88, Sec. 4, Ting-Chou Road, Taipei City, 11677, Taiwan  
Tel +886-2-77496722  
Fax +886-2-86631954  
Email nfchiu@ntnu.edu.tw

Chen-Yu Chen  
Department of Obstetrics and Gynecology, Mackay Memorial Hospital, No. 92, Sec. 2, Zhongshan N. Road, Taipei City, 10449, Taiwan  
Tel +886-2-25433535  
Fax +886-2-25433642  
Email f122481@mmh.org.tw

## Introduction

Advanced maternal age and late marriage have become a global trend,<sup>1</sup> and this phenomenon has led to an increase in maternal pregnancy diseases such as gestational diabetes, gestational hypertension and pre-eclampsia, and abnormal fetal diseases such as Down's syndrome (DS) and premature delivery or death. Many studies have confirmed that advanced maternal age is highly correlated with the incidence of fetal Down's syndrome (FDS), and thus these women are considered to be a high-risk group for DS.<sup>2-4</sup> DS remains the most common chromosomal abnormality (trisomy 21) disorder, and it is mostly sporadic and not genetic. The prevalence and life expectancy for people with DS have increased over the past 50 years.<sup>5,6</sup> Each year, about 6000 babies are born with DS, which is about 1 in every 700 babies born in the United States (2004–2006).<sup>7</sup> Between 1979 and 2003, the number of babies born with DS increased by about 31.1% in the United States.<sup>6</sup> Globally, the prevalence of DS in 2015 was 5,361,800 people,<sup>8</sup> with 26,500 deaths.<sup>9</sup> In addition, among the approximately 200,000 newborns born each year from 2005 to 2018 in Taiwan, an estimated 200 to 300 had DS. The prevalence of DS continues to increase as the maternal age increases; however, DS can be diagnosed by prenatal screening during pregnancy. In recent years, a highly sensitive and specific non-invasive prenatal blood test for DS during pregnancy using DNA<sup>10,11</sup> and serum biomarkers<sup>12-15</sup> has been introduced. The types of serum biomarkers can be divided into the first and second trimesters. For the first trimester (11–13 weeks) of pregnancy, a combined test for two early detectable serum markers, pregnancy-associated plasma protein A (PAPP-A) and human chorionic gonadotrophin (hCG) or its individual subunits (free  $\alpha$ -hCG and free  $\beta$ -hCG) has been shown to provide early diagnostic information with an assay rate of approximately 65%.<sup>12,13</sup> For the second trimester (14–18 weeks) of pregnancy, a double test for alpha-fetoprotein (AFP) and hCG has been shown to have an assay rate of 59%, compared to 69% for a triple test for AFP, hCG, and unconjugated estriol (uE), and 76% for a quadruple test for AFP, hCG, uE3, and inhibin A.<sup>14,15</sup> According to the current screening strategy, the overall detection rate of combined first and second trimester quadruple testing in Taiwan is between 80% and 85%.<sup>16</sup>

The maternal serum biomarker of pregnancy-associated plasma protein-A2 (PAPP-A2) has recently been used to screen for FDS<sup>17</sup> and pre-eclampsia.<sup>18</sup> PAPP-

A2 is a metalloproteinase that is similar to PAPP-A. The prepro-parts of PAPP-A2 and PAPP-A are not homologous, but mature PAPP-A2 shares 45% of its residues with PAPP-A.<sup>19</sup> The average PAPP-A2 level at the end of pregnancy (~200 ng/mL) is 500-fold higher than levels outside pregnancy (0.4 ng/mL).<sup>20</sup> In addition, the average PAPP-A level is about 25,000-fold higher in pregnant women (100 IU/mL at term) than in nonpregnant women (4 mIU/mL).<sup>20</sup> Interestingly, a previous study of DS diagnostic tests found that the serum concentration of PAPP-A decreased during the first trimester of pregnancy, and then increased during the second trimester, suggesting that PAPP-A2 can be used as a specific marker of DS.<sup>17,21</sup> In addition, Kløverpris et al reported an enzyme-linked immunosorbent assay (ELISA) for the detection of PAPP-A2 had a coefficient of variability of 20% at 0.08 ng/mL and a limit of detection (LOD) of 0.071 ng/mL.<sup>20</sup> Munnangi et al used sandwich ELISA to measure the concentration of PAPP-A2 in the serum of women with DS pregnancies, and reported a concentration of  $82.70 \pm 12.13$  ng/mL between 15 and 20 weeks in aneuploid pregnancies, and  $56.35 \pm 3.63$  ng/mL in normal pregnancies.<sup>17</sup> In addition, Bocková et al used a sandwich assay involving functionalized gold nanoparticle (AuNP)-based surface plasmon resonance (SPR) which could detect PAPP-A2 in 30% blood plasma at levels as low as 3.6 ng/mL.<sup>22</sup> In previous work, we showed that an SPR immunosensor based on functionalized graphene oxide (GO) could be used to detect PAPP-A2 at levels as low as 0.01 pg/mL in spiked human plasma.<sup>23</sup> In addition, Fan et al developed a GO-based SPR biosensor that allowed for the label-free simultaneous detection of PAPP-A and PAPP-A2 in clinical blood samples during pregnancy.<sup>24</sup> In addition, we demonstrated that a carboxyl-GO-based SPR aptasensor to assay hCG in the blood serum of pregnant women had a detection limit of 1.15 pM,<sup>25</sup> and that it could be used to screen women with fetal DS by detecting hCG protein at limits of 1 pM in buffer samples and 1.9 pM in clinical serum samples.<sup>26</sup>

To improve the sensitivity and LOD of biosensors for clinical application, novel types of graphene-like two-dimensional (2D) nanomaterials of molybdenum disulfide (MoS<sub>2</sub>) have been developed due to their extraordinary electronic structure, chemical bonding and optical properties. These 2D-MoS<sub>2</sub> materials have been proven to have high sensitivity and biocompatibility,<sup>27-37</sup> mainly through the beneficial biological effects and bioaffinity of sulfide in the material.<sup>38,39</sup> Furthermore, Sarkar et al

reported that a difference in band gap resulted in a more than 74-fold increase in sensitivity for MoS<sub>2</sub> over graphene.<sup>40</sup> Previous reports of MoS<sub>2</sub>-based biosensor technologies include electrochemical,<sup>27,28</sup> fluorescence,<sup>29</sup> field effect transistors,<sup>30–32,40</sup> SPR<sup>33–36</sup> and surface-enhanced Raman scattering<sup>37,41</sup> applications, mainly because of the high sensitivity, label-free quantification, accurate measurement and low cost for biomolecule detection. Soni et al used a polyaniline-MoS<sub>2</sub> hybrid nanostructure-based electrochemical biosensor to detect specific oligonucleotide DNA sequences in patients with chronic myelogenous leukemia, and reported an LOD of  $3 \times 10^{-18}$  M.<sup>27</sup> Chu et al used a thin-layer MoS<sub>2</sub> and graphene-based electrochemical sensor to detect circulating tumor DNA, and reported an LOD of  $1 \times 10^{-17}$  M and linear range from  $10^{-16}$  M to  $10^{-13}$  M.<sup>28</sup> Cai et al used a MoS<sub>2</sub>-based fluorescence biosensor for the detection of microRNA-21 in serum samples related to breast cancer, and reported an LOD of 500 pM.<sup>29</sup> Lee et al used a MoS<sub>2</sub>-based field effect transistor biosensor to electrically detect prostate-specific antigen, and reported an LOD of 1 pg/mL.<sup>30</sup> In addition, Liu et al used a MoS<sub>2</sub> field-effect transistor-based DNA sensor to screen for DS, and reported an LOD of 100 aM.<sup>32</sup> In our previous study, we developed a carboxyl-MoS<sub>2</sub>-based SPR immunosensor which exhibited high affinity to detect BSA and CK-19 proteins.<sup>33–35</sup> Few studies have reported the clinical application of MoS<sub>2</sub>-based SPR biosensors, and only focused on theoretical calculations<sup>42,43</sup> and spiked human serum analysis.<sup>34,35</sup> However, there have been no reports so far on the use of MoS<sub>2</sub>-based SPR biosensors to screen for diseases in clinical samples.

In this study, we fabricated a carboxyl-MoS<sub>2</sub>-based SPR biosensor to detect PAPP-A2 to screen for FDS in maternal serum samples. Our results showed effective biochemically amplified responses on the interfaces of Au and carboxyl-MoS<sub>2</sub> films. This interface feature is a new technology for surface plasmon-enhanced photocatalysis on metal-semiconductor heterostructures. A heterostructure interface with a high work function may increase the electric field efficiency and propagation energy state of surface plasmons to enhance performance and sensitivity. Carboxyl-MoS<sub>2</sub>-based SPR biosensors are of great significance and have high potential for use in clinical diagnosis applications due to the high sensitivity and bioaffinity of sulfide and the covalent targeting of the binding site carboxylic acid to detect biomolecules.

## Materials and Methods

### Preparation of Carboxyl-MoS<sub>2</sub> Nanocomposites and Carboxyl-MoS<sub>2</sub>-Based SPR Chips

MoS<sub>2</sub> powder (molybdenum (IV) sulfide, average particle size <2 μm, purity 98%, molecular weight 160.07) was purchased from Sigma-Aldrich (CAS 1317–33-5, 23,482) as shown in Figure 1A. In this study, MoS<sub>2</sub> sheets were prepared at a concentration of 2 mg/mL in a total volume of 15 mL deionized water using ultrasound-assisted liquid-phase exfoliation (UALPE) for 3 hours at 60°C and sonication power of 500 W as shown in Figure 1B. Then, 1.2 g of sodium hydroxide (NaOH) and 1.0 g of chloroacetic acid (ClCH<sub>2</sub>CO<sub>2</sub>H) were added to the MoS<sub>2</sub> sheet solution, followed by sonication for 3 hours to synthesize carboxyl-MoS<sub>2</sub> nanocomposites as shown in Figure 1C. As shown in a previous study,<sup>44</sup> the use of UALPE to prepare MoS<sub>2</sub> sheets can increase the amount of sulfur vacancies on the surface of MoS<sub>2</sub>. The mechanism of this modification facilitates the occupation of sulfur vacancies by the chlorine atoms of chloroacetic acid<sup>45,46</sup> to form covalent bond modifications as shown in Figure 1D. Finally, centrifugation was carried out using a 12,000 rpm centrifuge, and the supernatant (chloroacetic acid and NaOH) was replaced with deionized water to obtain a chloroacetic acid-modified aqueous solution of MoS<sub>2</sub>, which was termed carboxyl-MoS<sub>2</sub>. The synthesis of carboxyl-MoS<sub>2</sub> nanocomposites was pre-processed and improved based on previous work.<sup>33</sup>

To manufacture the sensor chip, we performed thermal evaporation deposition on a glass (BK7) substrate to obtain 2 nm chromium (Cr) and 47 nm gold (Au) thin films. The formation of short-chain amino alkane thiol molecule self-assembled monolayers (SAMs) was then achieved using 5 mM of cystamine dihydrochloride 98% (Cys) (C<sub>4</sub>H<sub>12</sub>N<sub>2</sub>S<sub>2</sub>, Alfa Aesar, United Kingdom) for 24 hours at room temperature to covalently bond amine groups onto the Au surface as shown in Figure 1D–F shows the carboxyl-MoS<sub>2</sub> nanocomposites at a concentration of 0.5 mg/mL to SAMs on the –NH<sub>2</sub> terminus of Cys to form chemical covalent bonds after 5 hours. This covalent immobilization can provide the best entry point to combine longevity of the carboxyl-MoS<sub>2</sub> modified surface with high sensitivity, resulting in the formation of three dimensional specific coordination sites,<sup>47</sup> which can facilitate the immobilization of antibodies.

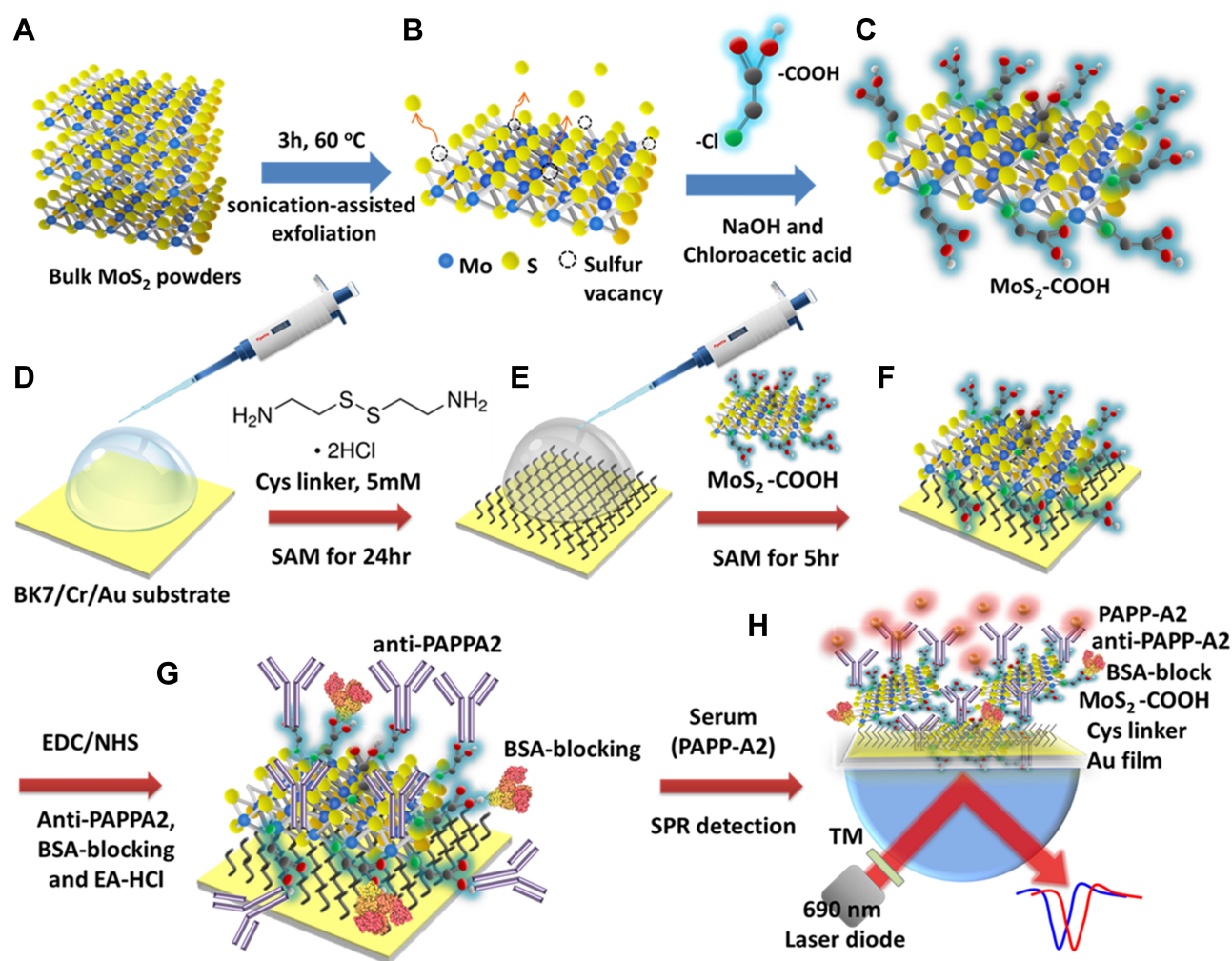


**Figure 1** Carboxyl-MoS<sub>2</sub> nanocomposite synthesis and the sensing mechanism of the carboxyl-MoS<sub>2</sub>-based SPR biosensor to detect PAPP-A2 protein in maternal serum samples. **(A)** Schematic diagram of sonication-assisted liquid-phase exfoliation (LPE) for the preparation of MoS<sub>2</sub> sheets. **(B)** MoS<sub>2</sub> exhibits a layered structure with planar Mo-S bonds and sulfur vacancies on the MoS<sub>2</sub> surface. **(C)** The carboxyl-MoS<sub>2</sub> nanocomposites were successfully modified by chloroacetic acid. Carboxyl-MoS<sub>2</sub>-based SPR chip immobilization steps and containing. **(D)** Au film substrate. **(E)** Cys linker containing a thiol-group to allow for assembly on the Au film substrate. **(F)** Covalent binding of carboxyl-MoS<sub>2</sub> on the Cys-linker. **(G)** EDC/NHS activated carboxyl groups resulting in a higher density of immobilized antibodies. **(H)** To detect PAPP-A2 protein to screen for Down's syndrome in maternal serum samples.

**Abbreviations:** MoS<sub>2</sub>, molybdenum disulfide; Carboxyl-MoS<sub>2</sub>, carboxyl-molybdenum disulfide; SPR, surface plasmon resonance; PAPP-A2, pregnancy-associated plasma protein-A2; Au, gold; Cys, cystamine; NH<sub>2</sub>, amine groups; EDC/NHS, 1-ethyl-3-(3-dimethylaminopropyl)carbodiimide/N-hydroxysuccinimide.

In this study, the modified carboxyl groups combined with the antibodies on the surface of MoS<sub>2</sub>, in which the lysine amine group coupled with the COOH group to form a covalent bond. We have analyzed the binding characteristics between COOH groups and antibodies in detail in previous studies.<sup>33,34</sup> These studies showed that the orientation of antibodies will affect the detection sensitivity. However, the present study used a high-density and three-dimensional method to modify the surface of MoS<sub>2</sub>-COOH to improve detection sensitivity.

We used an activator to activate the carboxylate group of the carboxyl-MoS<sub>2</sub> nanocomposites. This activator was composed of 1-ethyl-3-(dimethyl-aminopropyl) carbodiimide

hydrochloride (EDC, C<sub>8</sub>H<sub>17</sub>N<sub>3</sub>, Sigma-Aldrich, USA)/N-hydroxyl succinimide (NHS, C<sub>4</sub>H<sub>5</sub>NO<sub>3</sub>, Alfa Aesar, United Kingdom). For surface activation, we used an equal amount of 100 mL of a mixture of 0.1 M NHS and 0.4 M EDC pH 5.0–7.0 to activate the -COOH terminals of the carboxyl-MoS<sub>2</sub> surface. Carboxyl-MoS<sub>2</sub> sheets are strongly hydrophilic material, as they act as an acid and lose a proton to form a negatively charged carboxylate ion on the MoS<sub>2</sub> surface, which facilitates the immobilization of antibodies. For the immunoassay, antibody proteins of anti-PAPP-A2 (MBS690059, mouse anti-human pappalysin-2 monoclonal antibody, molecular mass of 150 kDa, MyBioSource, USA) were immobilized on the carboxyl-MoS<sub>2</sub> surface for 4 hours

at 4°C. The  $-NH_2$  present in the lysine amino acid side-chain on the anti-PAPPA2 protein (25  $\mu\text{g}/\text{mL}$ ) surface can be used for covalent immobilization in a random fashion on the carboxyl-MoS<sub>2</sub> surface. This was followed by the addition of 100 mg/mL bovine serum albumin (BSA, pH 7,  $\geq 98\%$ , CAS 9048-46-8, B4287, Sigma-Aldrich, USA) to block the remaining (other unbound antibodies)  $-COOH$  bonds. The reaction was then terminated by dissolving 1 M ethanolamine hydrochloride (EA-HCl,  $\geq 99.0\%$ , CAS 2002-24-6, Sigma-Aldrich, USA) in phosphate-buffered saline (PBS) to deactivate unreacted carboxyl groups, which effectively reduced non-specific binding as shown in Figure 1G.

In this study, we performed all immunoassay reactions using a BI-SPR 3000 dual-channel system (Biosensing Instrument Inc., Arizona, USA). The reference channel compensated for temperature drift and also the bulk index of refraction shifts and non-specific signals. This allowed for the label-free and rapid detection of PAPP-A2 with the carboxyl-MoS<sub>2</sub>-based SPR chip in clinical serum samples. All of the sample injections used a flow rate of 60  $\mu\text{L}/\text{minute}$  and volume of 200  $\mu\text{L}$  at room temperature as shown in Figure 1H.

## Preparation of Running Buffers and Clinical Blood Samples

The preparation of a running buffer for clinical use is a very important experimental parameter in the detection of serum samples, as it can reduce false-positive reactions caused by non-specific binding. Our running buffer has been optimized for carboxyl-MoS<sub>2</sub>-based SPR biosensors involving serum protein immunoassays. This non-specific binding is primarily caused by molecular interactions between the serum analyte (such as plasma proteins, peptides, fats, carbohydrates, growth factors, hormones, inorganic substances) and the sensor surface (such as charge interactions, hydrophilic interactions, and Van der Waals force). In order to reduce and eliminate non-specific interactions of the analysis proteins and carboxyl-MoS<sub>2</sub> surface, we used running buffer for clinical conditions of 1 mg/mL (600  $\mu\text{L}$ ) BSA, 50 mM NaCl (500  $\mu\text{L}$ ), and 0.05% (50  $\mu\text{L}$ ) non-ionic surfactant Tween-20 (1 g/mL, P9416, Sigma-Aldrich, USA) combined with experimental conditions in 1x (100 mL) PBS to cause an interfacial negative charge and disrupt hydrophobic interactions. We adjusted the pH of the buffer to approximately 7.0–7.5 and defined it as PBS<sub>BNT</sub> buffer for the clinical assay. The

PBS<sub>BNT</sub> buffer was used to dilute the serum sample and as a running buffer for the carboxyl-MoS<sub>2</sub>-based SPR biosensor experiments.

For the serum samples, we used maternal serum samples from normal pregnant women (NPW) and from pregnant women with FDS provided by attending physician Dr. Chen-Yu Chen from Mackay Memorial Hospital. There were 10 FDS and 4 NPW samples of maternal serum blood: at 19 weeks (FDS-1), 20 weeks (FDS-2), 14 weeks (FDS-3), 14 weeks (FDS-4), 22 weeks (FDS-5), 19 weeks (FDS-6), 21 weeks (FDS-7), 18 weeks (FDS-8), 19 weeks (FDS-9), and 18 weeks (FDS-10), and 14 weeks (NPW-1), 12 weeks (NPW-2), 14 weeks (NPW-3) and 16 weeks (NPW-4), respectively. All 14 clinical samples were collected from Taiwanese pregnant women, and the FDS and NPW groups are shown in Tables S1 and S2, respectively, including age, history of miscarriage and when blood was drawn. The concentrations of PAPP-A2 in the serum samples were measured using a Human Pappalysin 2 (PAPP-A2) ELISA Kit Sandwich (MBS724290, MyBioSource, California, USA), and were 95.15, 84.75, 74.27, 108.84, 86.26, 63.92, 56.74, 77.28, 52.96, 63.74, 25.52, 32.67, 38.97 and 23.50 ng/mL, respectively. In the statistical analysis, we used the Student's *t* test and Fisher's exact test to compare correlations between maternal age, time of miscarriage and SPR angle shifts of the serum diluted in clinical samples.

This study was conducted in accordance with the Declaration of Helsinki Ethical Principles. All experiments were performed in compliance with the relevant laws and institutional guidelines, and the work was approved by the Institutional Review Board (IRB) of Mackay Memorial Hospital for Human Clinical Trials (Permit Numbers: 15MMHIS020, 15MMHIS115 and 17MMHIS185). Informed consent was obtained from all of the enrolled women for the collection and examination of clinical samples. All personal identifiers were anonymized prior to analysis. This manuscript does not involve mouse cell line experiments.

## Results and Discussion

### Morphology and Elemental Analysis of Carboxyl-MoS<sub>2</sub> Nanocomposites

The carboxyl-MoS<sub>2</sub> nanocomposites were analyzed using scanning electron microscopy (SEM) and transmission electron microscopy (TEM) and energy dispersive X-ray spectroscopy (EDS). A micrograph of the carboxyl-MoS<sub>2</sub> sheets

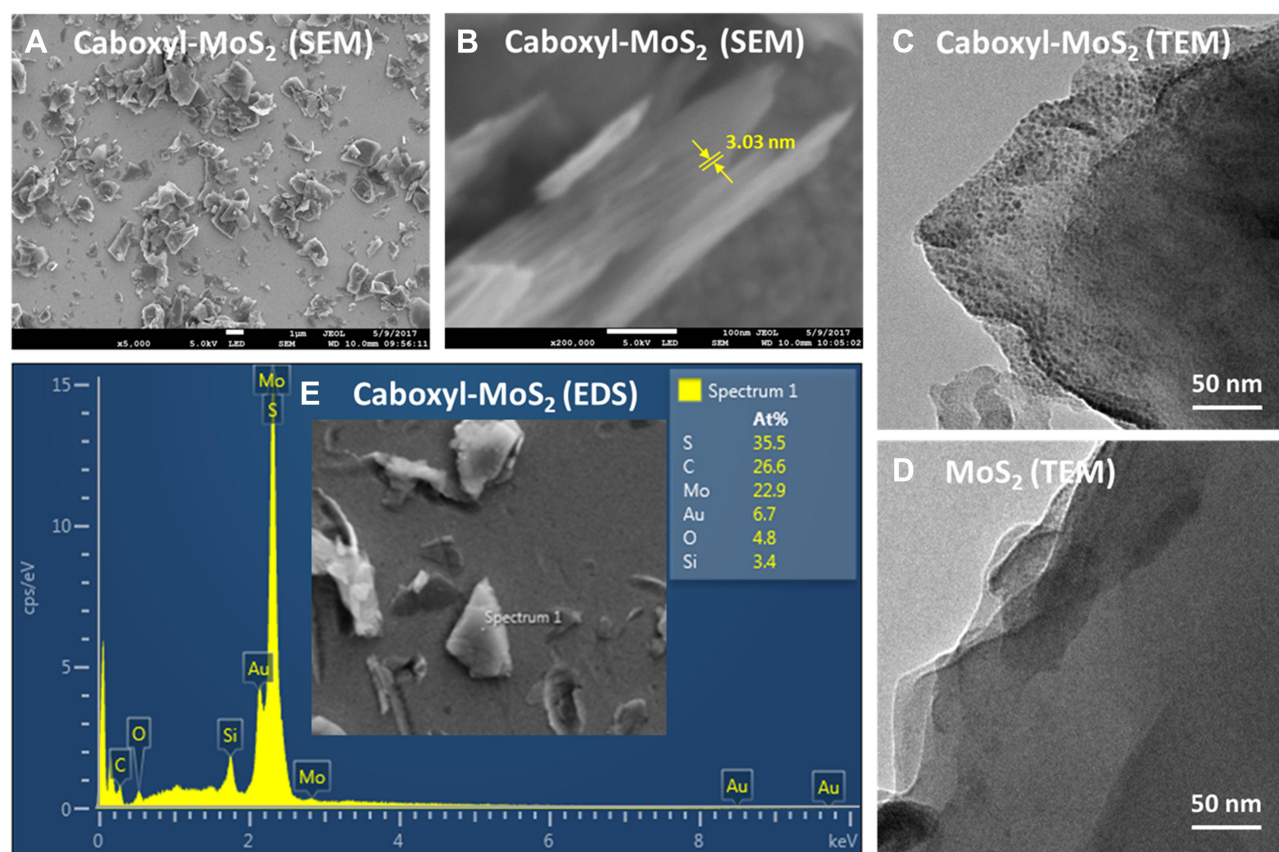


**Figure 2** (A) SEM image of carboxyl-MoS<sub>2</sub> sheets. (B) Cross-sectional SEM image of lateral flake thickness of carboxyl-MoS<sub>2</sub> sheets. (C) TEM image of the carboxyl-MoS<sub>2</sub> sheets. (D) TEM image of the MoS<sub>2</sub> sheets. (E) EDS analysis of the carboxyl-MoS<sub>2</sub> sheets (insert shows the carboxyl-MoS<sub>2</sub> sheet for the EDS analysis). **Abbreviations:** MoS<sub>2</sub>, molybdenum disulfide; Carboxyl-MoS<sub>2</sub>, carboxyl-molybdenum disulfide; SEM, scanning electron microscopy; TEM, transmission electron microscopy; EDS, energy dispersive X-ray spectroscopy.

showed 2D flakes with grain boundaries and stacking order structures. SEM micrographs of the carboxyl-MoS<sub>2</sub> sheets on the BK7/Cr/Au chip surface are shown in Figure 2A and B. Figure 2A shows that the carboxyl-MoS<sub>2</sub> sheet had an average size <2 μm, and Figure 2B shows a cross-sectional SEM image of multi-layered MoS<sub>2</sub> sheets with a flake thickness of 3.03 nm.

Figure 2C and D show high-resolution TEM images of the surfaces of the carboxyl-MoS<sub>2</sub> and MoS<sub>2</sub> sheets. Compared to the MoS<sub>2</sub> sheets, the surface morphology of the carboxyl-MoS<sub>2</sub> sheets at the carboxylic acid formed a typical organic chitosan matrix compound shape with a hydrophilic surface, which is similar to previous studies.<sup>33,34,48,49</sup> Figure 2E shows the EDS element analysis of the BK7/Au/carboxyl-MoS<sub>2</sub> chip. The spectrum showed sulfur (S), carbon (C), molybdenum (Mo), gold (Au), oxygen (O) and silicon (Si) element content peaks of 35.5, 26.6, 22.9, 6.7, 4.8, and 3.4, respectively. The EDS spectrum exhibited strong S (K<sub>α</sub>) and Mo (L<sub>α</sub>) peaks, which is in agreement with the S to Mo atomic ratio of

about 1.55, indicating sulfur vacancies in the carboxyl-MoS<sub>2</sub> sheets. These results proved that chloroacetic acid had successfully modified the carboxyl-MoS<sub>2</sub> nanocomposites.

## XPS Spectra of Carboxyl-MoS<sub>2</sub> and MoS<sub>2</sub> Sheets

Representative X-ray photoelectron spectroscopy (XPS) spectra of MoS<sub>2</sub> (Figure 3A) and carboxyl-MoS<sub>2</sub> (Figure 3B) clearly showed elemental signals of Mo, C, O, S, Si and Au, where Si and Au were due to the glass and gold substrate composition.

The Mo(3d<sub>5/2</sub>):S(2p) ratios of MoS<sub>2</sub> and carboxyl-MoS<sub>2</sub> were calculated from the peak areas of the XPS patterns as 1:1.36 and 1:1.27, respectively, indicating the sulfur-vacancy-enriched structures of carboxyl-MoS<sub>2</sub>.

The presence of Cl 2p signals in the MoS<sub>2</sub> and carboxyl-MoS<sub>2</sub> sheets were investigated using high-resolution XPS spectra as shown in Figure 3C. The MoS<sub>2</sub> sheets were modified by chloroacetic acid to form a chlorine atom on the surface that replaced the sulfur

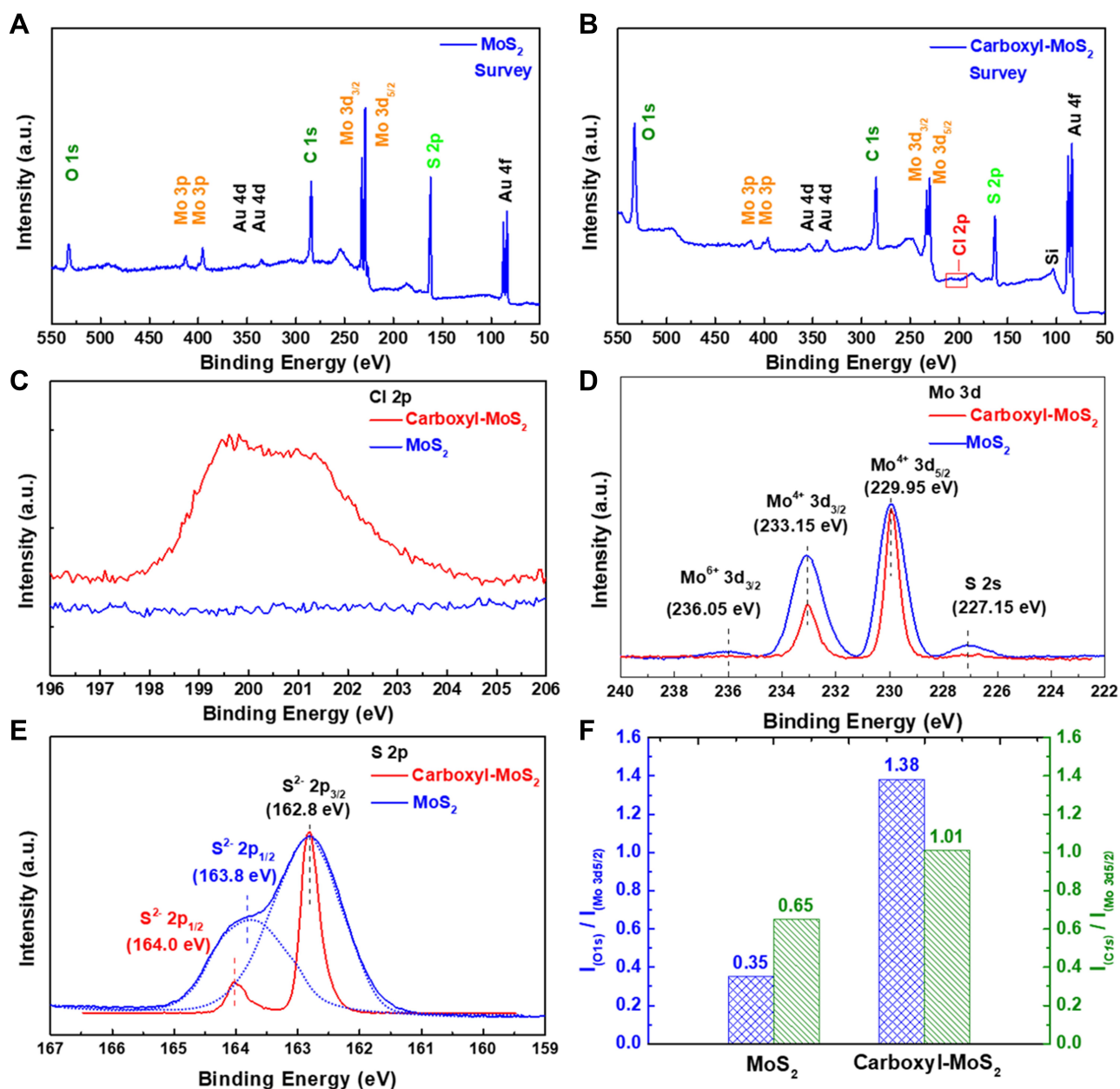


**Figure 3** The XPS survey spectra of (A) MoS<sub>2</sub> sheets and (B) carboxyl-MoS<sub>2</sub> sheets. The high-resolution XPS spectra of (C) Cl 2p, (D) Mo 3d, (E) S 2p for MoS<sub>2</sub> and carboxyl-MoS<sub>2</sub> sheets. (F) Analysis of XPS surface atomic intensity ratios of C1s/Mo3d and O1s/Mo3d on MoS<sub>2</sub> and carboxyl-MoS<sub>2</sub> sheets.

**Abbreviations:** MoS<sub>2</sub>, molybdenum disulfide; Carboxyl-MoS<sub>2</sub>, carboxyl-molybdenum disulfide; XPS, X-ray photoelectron spectroscopy.

atom. Accordingly, the presence of chlorine atoms (Cl 2p) was detected on the XPS spectra, signifying that most of the carboxyl modification on the MoS<sub>2</sub> surface was arranged in the structure. This result indicated that the modification of the carboxyl-MoS<sub>2</sub> nanocomposites was successful.

We also used XPS to analyze the binding energies of Mo 3d and S 2s in the MoS<sub>2</sub> and carboxyl-MoS<sub>2</sub> sheets as shown in Figure 3D. The same vibration orbitals of Mo<sup>4+</sup> in the MoS<sub>2</sub> and carboxyl-MoS<sub>2</sub> sheets were observed

from the binding energy of Mo 3d<sub>3/2</sub> and Mo 3d<sub>5/2</sub> doublet peaks. The two strong doublets at binding energies of 233.15 and 229.95 eV corresponded to the binding energies of Mo 3d<sub>3/2</sub> and Mo 3d<sub>5/2</sub>, respectively, indicating that Mo<sup>4+</sup> species were dominant in the product. The intensity of the Mo<sup>4+</sup> 3d<sub>3/2</sub> peak was lower in the carboxyl-MoS<sub>2</sub> sheets, suggesting higher carboxylic surface coverage. In addition, the peak at a binding energy of 227.15 eV could be indexed as S 2s, and the Mo 3d<sub>3/2</sub> peak at 236.05 eV showed that the peak was attributed to the Mo<sup>6+</sup> state in

MoS<sub>2</sub>. The decrease in intensity of the S 2s and the Mo<sup>6+</sup> 3d<sub>3/2</sub> peaks in the carboxyl-MoS<sub>2</sub> sheets may have been affected by structural changes caused by carboxyl modification.

In addition, the existence of S 2p orbitals of sulfur species in the MoS<sub>2</sub> and carboxyl-MoS<sub>2</sub> sheets were observed from the binding energies of S<sup>2-</sup> 2p<sub>1/2</sub> and S<sup>2-</sup> 2p<sub>3/2</sub> orbitals as shown in Figure 3E. In the MoS<sub>2</sub> sheet, S<sup>2-</sup> 2p located at 163.8 and 162.8 eV could be assigned to the spectra of S<sup>2-</sup> 2p<sub>1/2</sub> and S<sup>2-</sup> 2p<sub>3/2</sub> orbitals.<sup>50–52</sup> In comparison, in the carboxyl-MoS<sub>2</sub> sheet, the S<sup>2-</sup> 2p spectrum showed two binding energy peaks at 162.8 eV (S 2p<sub>3/2</sub>) and 164.0 eV (S 2p<sub>1/2</sub>). This result showed that the binding energy of S 2p in the carboxyl-MoS<sub>2</sub> sheet had a larger forward shift, indicating that it was caused by carboxyl modification, and signifying the oxidation state in the carboxy-MoS<sub>2</sub> heterostructure.<sup>53,54</sup>

In XPS analysis (Figure 3A and B), intensity ratios of O(1s)/Mo(3d<sub>5/2</sub>) and C(1s)/Mo(3d<sub>5/2</sub>) atomic ratios in the MoS<sub>2</sub> sheet were 0.35 and 0.65, respectively, compared to 1.38 and 1.01 in the carboxyl-MoS<sub>2</sub> sheets. This confirmed that the carboxyl modification of MoS<sub>2</sub> had successfully increased the carbon and oxygen content of the MoS<sub>2</sub> surface. As a result, the ratios of the intensity of O(1s)/Mo(3d<sub>5/2</sub>) and C(1s)/Mo(3d<sub>5/2</sub>) peaks showed that carboxyl-MoS<sub>2</sub> had a relative increase in carbon and oxygen content compared to MoS<sub>2</sub> (Figure 3F).<sup>55</sup>

## XPS and UPS Spectroscopy Analysis of the Interface Energy and Elements of the Carboxyl-MoS<sub>2</sub> Sheets

Figure 4A and B show the deconvoluted C1s and O1s peaks of the surface of the carboxyl-MoS<sub>2</sub> sheets. The carboxyl-MoS<sub>2</sub> sheets displayed multiple C1s peaks, ranging from 284.6 to 288.6 eV (Figure 4A). The higher peaks at 284.6, 286.5 and 288.6 eV could be ascribed to non-oxygenated ring (C-C) bonds, hydroxyl carbon (C-O) bonds and carboxylate carbon (O-C=O) bonds, respectively. Three peaks were identified in the O1s spectra that corresponded to carbonyl carbon (C=O, 531.4 eV) bonds, C-O bonds (532.7 eV), and O-C=O bonds (533.2 eV) as shown in Figure 4B. In addition, high-resolution C1s and O1s spectra indicated the presence of O=C-O bond contents at C1s and O1s of 24.4% and 28.2%, respectively, in the carboxyl-MoS<sub>2</sub> sheets. The mass percentages of C and O were calculated according to the XPS results, and showed that the carboxyl-modified

MoS<sub>2</sub> had a much higher content of C and O, further confirming the successful attachment of carboxylic groups.<sup>55</sup>

We then used ultraviolet photon spectroscopy (UPS) to explore the energy level alignment with respect to the work function ( $\Phi$ ) (Figure 4C). We performed work function analysis in order to understand the characteristics of the interface electric field of the MoS<sub>2</sub> and carboxyl-MoS<sub>2</sub> interfaces. Our experimental UPS measurements were performed in an ultra-high vacuum chamber using a helium light source. The work function was calculated as  $\Phi = hv - E_C - E_F$ , where  $hv$  is the incident photon energy (21.2 eV).<sup>23,51,52</sup> The MoS<sub>2</sub> and carboxyl-MoS<sub>2</sub> sheets were separately immobilized on BK7 substrates coated with 47 nm of Au film. As shown in Figure 4C, the binding energies of Au, Au/MoS<sub>2</sub> and Au/carboxyl-MoS<sub>2</sub> in the layer-by-layer material surface were 16.1, 17.0 and 16.5 eV, respectively. According to these calculations, the Au, MoS<sub>2</sub> and carboxyl-MoS<sub>2</sub> work functions were 5.1, 4.2 and 4.72 eV, respectively. The UPS clearly showed the work function of the MoS<sub>2</sub> and carboxyl-MoS<sub>2</sub> sheets, confirming the creation of heterojunctions between Au/MoS<sub>2</sub> and Au/carboxyl-MoS<sub>2</sub>, where the Au film was used as a reference electrode.

The energy band diagrams of MoS<sub>2</sub> and carboxyl-MoS<sub>2</sub> relative to the work function of Au film are illustrated in Figure 4D and E. Comparing the energy band diagrams of Figure 4D and E, the energy separation  $\Delta E$  between the conduction band of carboxyl-MoS<sub>2</sub> and the EF of Au was small. The higher work function was possibly correlated with the carboxylic acid groups at the edges of MoS<sub>2</sub>. This high work function may thus improve the efficiency of the electric field and propagation energy state of the surface plasmon.<sup>56,57</sup> This interface feature is a new technology for surface plasmon-enhanced photocatalysis using metal-semiconductor heterostructures.<sup>58,59</sup>

## Captured Antibodies Were Immobilized on the Chip Surface and Pre-Analytic Sample Processing

The capture of anti-PAPP-A2 proteins on the carboxyl-MoS<sub>2</sub>-based SPR biosensor was examined using real-time observations of specific molecular dynamic interactions as shown in Figure 5. This experiment evaluated and analyzed clinical serum samples to study the equilibrium constant of the antigen-antibody interactions using an immunoassay, which is conducive to the immobilization



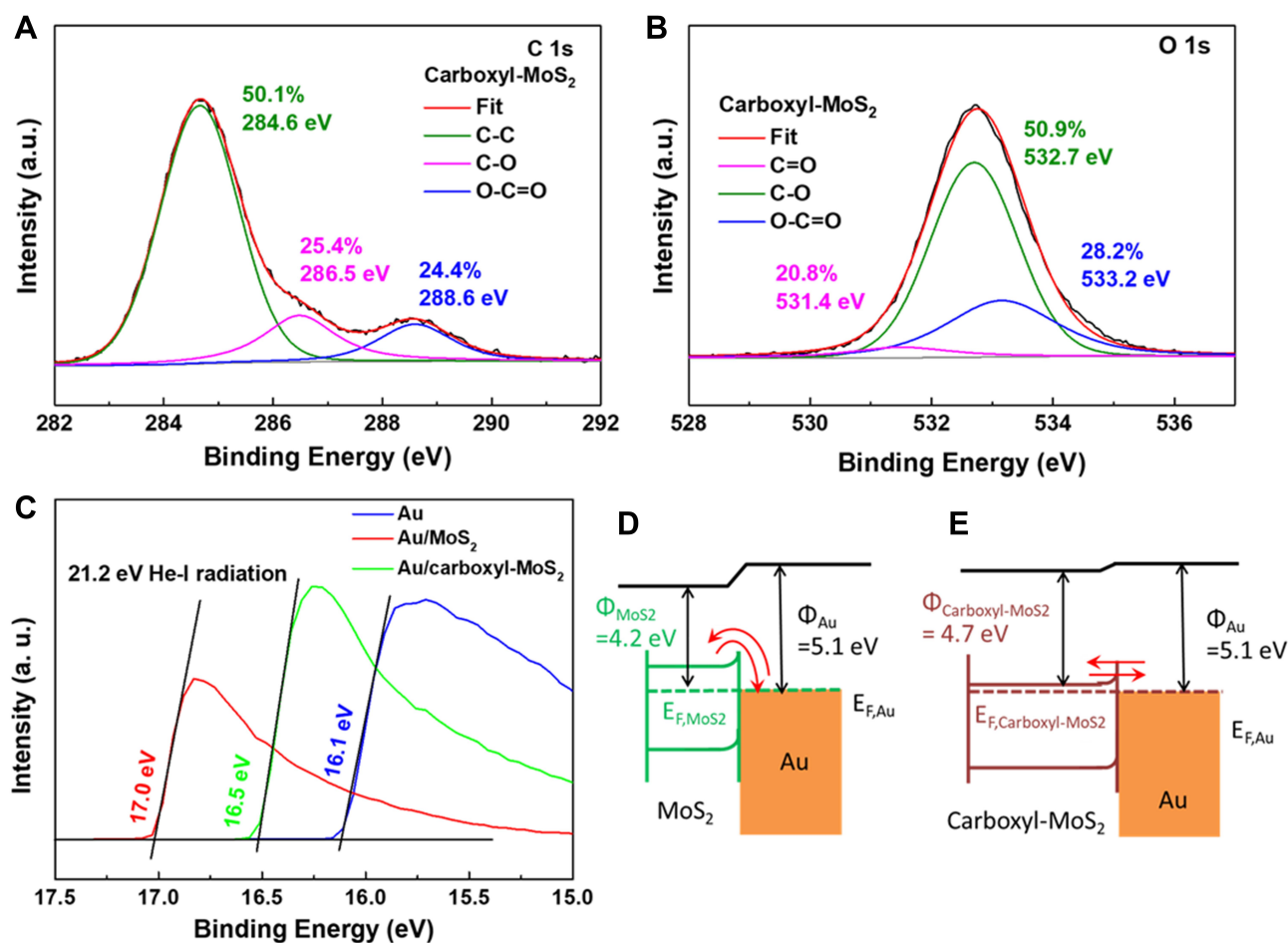


**Figure 4** High energy resolution XPS spectra of (A) C1s and (B) O1s regions on carboxyl-MoS<sub>2</sub> sheets. (C) UPS spectra of different interfaces of Au, Au/MoS<sub>2</sub> and Au/carboxyl-MoS<sub>2</sub> film. Band diagram of (D) Au/MoS<sub>2</sub> and (E) Au/carboxyl-MoS<sub>2</sub> heterojunctions obtained from UPS measurements. The band-gap energies used in the diagram are optical gaps.

**Abbreviations:** MoS<sub>2</sub>, molybdenum disulfide; Carboxyl-MoS<sub>2</sub>, carboxyl-molybdenum disulfide; Au, gold; XPS, X-ray photoelectron spectroscopy; UPS, ultraviolet photon spectroscopy.

of antibodies and the optimization of the recognition mechanism of the tested molecules in the serum. The flow rate was first set to 60  $\mu\text{L}/\text{min}$  with an injection volume of 200  $\mu\text{L}$  of EDC/NHS to activate the carboxyl-MoS<sub>2</sub> surface functional groups. For the immobilization of antibodies, in order to increase the amount of protein bound to the surface of the chip, we reduced the flow rate to 10  $\mu\text{L}/\text{min}$  and 25  $\mu\text{g}/\text{mL}$  of anti-PAPP-A2 and 1  $\text{mg}/\text{mL}$  of BSA were injected. The purpose of immobilizing BSA is to reduce the adsorption of non-specific molecules on the surface of the chip.<sup>25,26,34</sup> Figure 5A shows that the anti-PAPP-A2 resonance angle reached about 221.56 millidegrees ( $\text{m}^\circ$ ) at 2500 sec, and increased to 268.83  $\text{m}^\circ$  at 4500 sec after BSA injection. We then used a high flow rate of 60  $\mu\text{L}/\text{min}$  and injected 10 mM of NaOH to remove unbound protein (anti-PAPP-A2 and BSA). Next, 1 M high concentration EA-HCl was injected

to halt the remaining functional group interface activation.<sup>60–62</sup> Finally, another 10 mM of NaOH was injected and the chip immobilization procedure was completed. After the flow rate had been adjusted to 60  $\mu\text{L}/\text{min}$  and NaOH had been injected for the second time, the resonance angle dropped to 154.95  $\text{m}^\circ$ , which showed the true resonance angle of anti-PAPP-A2 and BSA proteins.

In previous work,<sup>33,34</sup> we reported the results of traditional SPR and carboxyl-MoS<sub>2</sub>-based SPR chips with regards to antibody concentration immobilization conditions used to measure molecular interactions and SPR angle shifts between chip surfaces. For antibody binding to BSA immobilized on carboxyl-MoS<sub>2</sub>,<sup>33</sup> the carboxyl-MoS<sub>2</sub>-based SPR biosensor had a 3.1-fold increase in SPR angle response compared to the traditional SPR chip. For antibody binding to CYFRA21-1 immobilized on

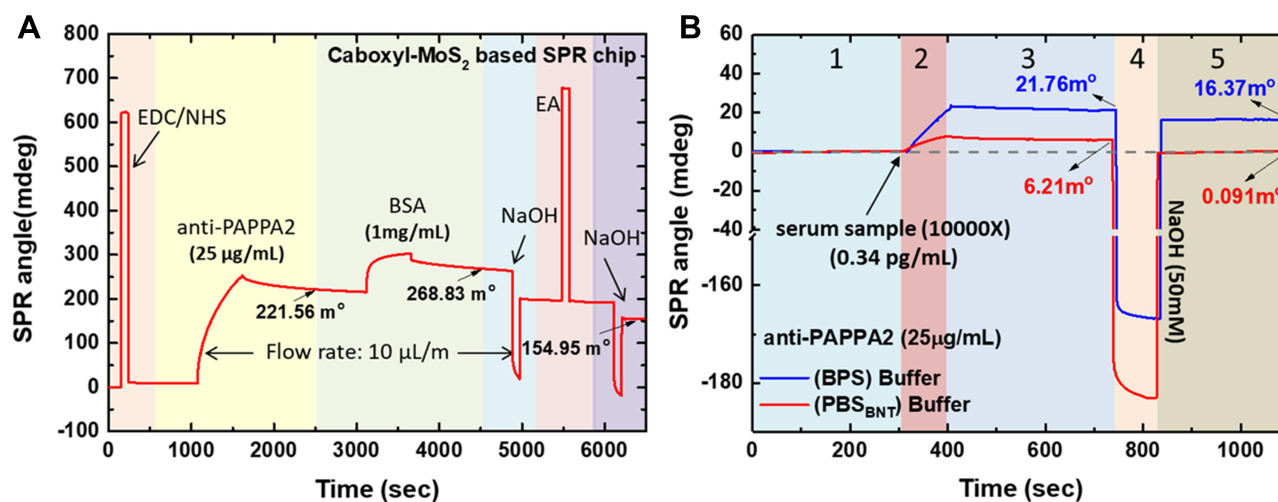


**Figure 5** (A) Optimization of the immobilization process of antibodies in carboxyl-MoS<sub>2</sub>-based SPR chips. (B) Non-specific molecular dissociation reactions were tested using PBS and PBS<sub>BNT</sub> buffer, respectively.

**Abbreviations:** Carboxyl-MoS<sub>2</sub>, carboxyl-molybdenum disulfide; SPR, surface plasmon resonance; PBS, phosphate-buffered saline; PBS<sub>BNT</sub>, phosphate-buffered saline (BSA, NaCl, Tween-20).

carboxyl-MoS<sub>2</sub>,<sup>34</sup> the carboxyl-MoS<sub>2</sub>-based SPR biosensor had a 2.6-fold increase in SPR angle response compared to the traditional SPR chip. With regards to the immobilization and quantitative analysis, the results showed that a carboxyl-MoS<sub>2</sub>-based SPR chip was superior to a traditional SPR chip with regards to interactions with protein molecules. This proves that the three-dimensional coordination sites of a carboxyl-MoS<sub>2</sub>-based SPR chip are superior to a conventional SPR chip. Carboxyl group modification has good binding ability and the advantage of orientation steric hindrance.

To evaluate the non-specific assay of the chip surface, we diluted the serum sample 10,000-fold (the concentration of PAPP-A2 was 0.34 pg/mL) and analyzed the non-specific binding reaction during the immunoassay as shown in Figure 5B. The serum sample was injected at a flow rate of 60 µL/min at 300 sec, and running buffer was immediately injected at 400 sec with NaOH at 750 sec. As shown in Figure 5B, when PBS (1X) was used as the running buffer (blue curve), the results were non-specific (antigen-antibodies could not dissociate or regenerate). When PBS<sub>BNT</sub> buffer was used as the running buffer (red curve) with injection of the same serum sample followed by NaOH for regeneration, the results showed that PBS<sub>BNT</sub> buffer could return to the original reference position at baseline. The experimental results showed that the response angles of the blue and red curves were 21.76 m° and 6.21 m°, respectively. Therefore, the addition of BSA, Tween-20, and NaCl in the running buffer

(PBS<sub>BNT</sub> buffer) and samples could effectively reduce the influence of non-specific molecule binding on the SPR detection immunoassay. Among them, BSA and Tween-20 can disrupt ionic and hydrophobic biomolecule-surface bonds,<sup>23,25,26</sup> and NaCl can disrupt the charge interactions between a protein and carboxyl surface to reduce non-specific binding.<sup>34</sup> Furthermore, adjusting the pH of the sample and running buffer (PBS<sub>BNT</sub> buffer) can alter the protein's isoelectric point range (predicted neutral overall charge) to reduce the influence of non-specific binding.

### Assay of PAPP-A2 Protein in Maternal Serum Using the Carboxyl-MoS<sub>2</sub>-Based SPR Biosensor

To evaluate the PAPP-A2 protein assay, we used maternal serum samples from NPW and pregnant women with FDS. All serum samples were taken from the upper layer of the blood and diluted with PBS<sub>BNT</sub> buffer at dilution factors of 100-fold, 500-fold, 1k-fold, 5k-fold, 10k-fold, 30k-fold, and 40k-fold. The binding reaction of PAPP-A2 in the serum was detected in the different diluted serum samples, and 60 µL/min of running buffer (PBS<sub>BNT</sub> buffer) was injected to wash unbound molecules after 90 sec of the reaction. Surface regeneration at the end of each analyte concentration assessment was performed at 200 sec after the injection of 12.0 pH NaOH at a flow rate of 60 µL/min. The NaOH buffer was used to remove any residual serum sample and dissociate antigen-antibody interactions from the surface of the sensor chip.

Figure 6 shows the SPR response analysis of the sensorgram curves obtained by measuring the 10 serum samples of the FDS group in whom blood was drawn at different weeks to detect PAPP-A2 protein concentration. The sensorgram curves of the FDS group at different serum dilutions are shown in Figure 6A–J. Figure 6A shows the FDS-1 (19 weeks) serum concentrations diluted 100-fold (951.50 pg/mL), 500-fold (190.30 pg/mL), 1k-fold (95.15 pg/mL), 5k-fold (19.03 pg/mL), 10k-fold (9.52 pg/mL), 30k-fold (3.17 pg/mL), and 40k-fold (2.38 pg/mL) had relative SPR angle shifts of 119.24, 73.90, 53.18, 17.22, 5.81, 3.77 and 3.63 m°, respectively. For detailed information of the FDS group in Figure 6 (the relationship between the SPR angle and the dilution ratio and concentration of serum PAPP-A2), please refer to Table S1.

Figure 7 shows the SPR response analysis of the sensorgram curves obtained by measuring four serum samples from healthy women (NPW group) in whom blood was drawn at different weeks to detect PAPP-A2 protein concentration. Figure 7A–D show that in the serum diluted by 100-fold, the serum PAPP-A2 concentrations in the NPW-1, NPW-2, NPW-3, and NPW-4 samples were 255.20, 326.74, 389.70, and 235.02 pg/mL, corresponding to SPR angle shifts of 42.77, 43.78, 46.57, and 40.96 m°, respectively. Detailed information of the relationships between the concentrations of PAPP-A2 and SPR angle shifts of detected PAPP-A2 protein in the maternal serum samples at different dilutions on the carboxyl-MoS<sub>2</sub>-based SPR biosensor are shown in Table S1 for the FDS group and Table S2 for the NPW group.

Therefore, we could clearly see that under the same dilution factor, the SPR angle shift in the NPW group was smaller than that in the FDS group. This is because the concentration of PAPP-A2 in the serum was lower in the NPW group than in the FDS group. We further analyzed these results at different serum dilution factors, and compared the sensitivity between the carboxyl-MoS<sub>2</sub>-based SPR chip and commercial ELISA kits as shown in Figure S1. Compared with ELISA kits, the carboxyl-MoS<sub>2</sub>-based SPR chip has higher sensitivity. Both methods (SPR and ELISA) showed acceptable results to detect PAPP-A2 in the serum of the NPW and FDS groups, with different linear regression and correlations with each other as shown in Figure S1A–S1F.

The linear regression equation for the serum diluted by 100-fold was  $y = 1.14x + 14.03$  with a correlation coefficient ( $R^2$ ) of 0.95, where  $x$  is the analyte concentration

(ELISA) in serum, and  $y$  is the SPR angle shift (m°) as shown in Figure S1A. Figures S1B–F show dilutions of the serum samples at 500-fold, 1k-fold, 5k-fold, 10k-fold, and 30k-fold, respectively. The linear regression equations of the calibration curves were  $y = 0.33x + 0.85$  ( $R^2 = 0.82$ ) for 500-fold,  $y = 0.46x - 1.43$  ( $R^2 = 0.79$ ) for 1k-fold,  $y = 0.54x + 3.59$  ( $R^2 = 0.59$ ) for 5k-fold,  $y = 0.45x + 2.89$  ( $R^2 = 0.24$ ) for 10k-fold, and  $y = 0.42x + 2.15$  ( $R^2 = 0.07$ ) for 30k-fold. Overall, as shown in Figure S1, when diluted by 10k- and 30k-fold, the correlation  $R$  square values were only 0.24 and 0.07, respectively, which were relatively lower than the low dilution samples. There was a good correlation between the results obtained from the SPR sensor and ELISA measurements of the PAPP-A2 levels at 100-fold dilution. The experiment results showed that the greater the dilution of the serum, the worse the linear regression equation and the correlation coefficient.

In addition, the SPR angle shift measured at a high dilution rate (5k- to 30k-fold) was very small. This is because the use of a high dilution ratio resulted in a relative decrease in the PAPP-A2 protein concentration in the serum. Therefore, we could clearly see that the dilution ratio of serum was more than 5k-fold, which resulted in no linearity. In this study, we tried to reduce interference and non-specific adsorption and achieve reasonable and accurate screening results, and thereby significantly increase the lower concentration assay of carboxyl-MoS<sub>2</sub>-based SPR chips. Regarding the dilution factor, the higher the sample dilution factor, the lower the interference and non-specific adsorption of other molecules in the serum. Therefore, the more diluted the sample, the lower the PAPP-A2 concentration in the sample, which reduced the sensitivity and linearity. In addition, a lower dilution rate of a sample increased the interference and nonspecific adsorption.<sup>23</sup>

## Quantitative Analysis of Calibration Curves and Specificity for FDS Screening Assay

Figure 8A shows the ELISA calibration curves for 10-fold dilution of the pregnant women's serum generated using a quantitative sandwich ELISA kit test. The results showed goodness of fit between ELISA responses obtained upon interactions of different concentrations of serum PAPP-A2 protein with antibodies immobilized on the surface of the ELISA wells. Calibration curves for PAPP-A2 protein were obtained at concentrations ranging

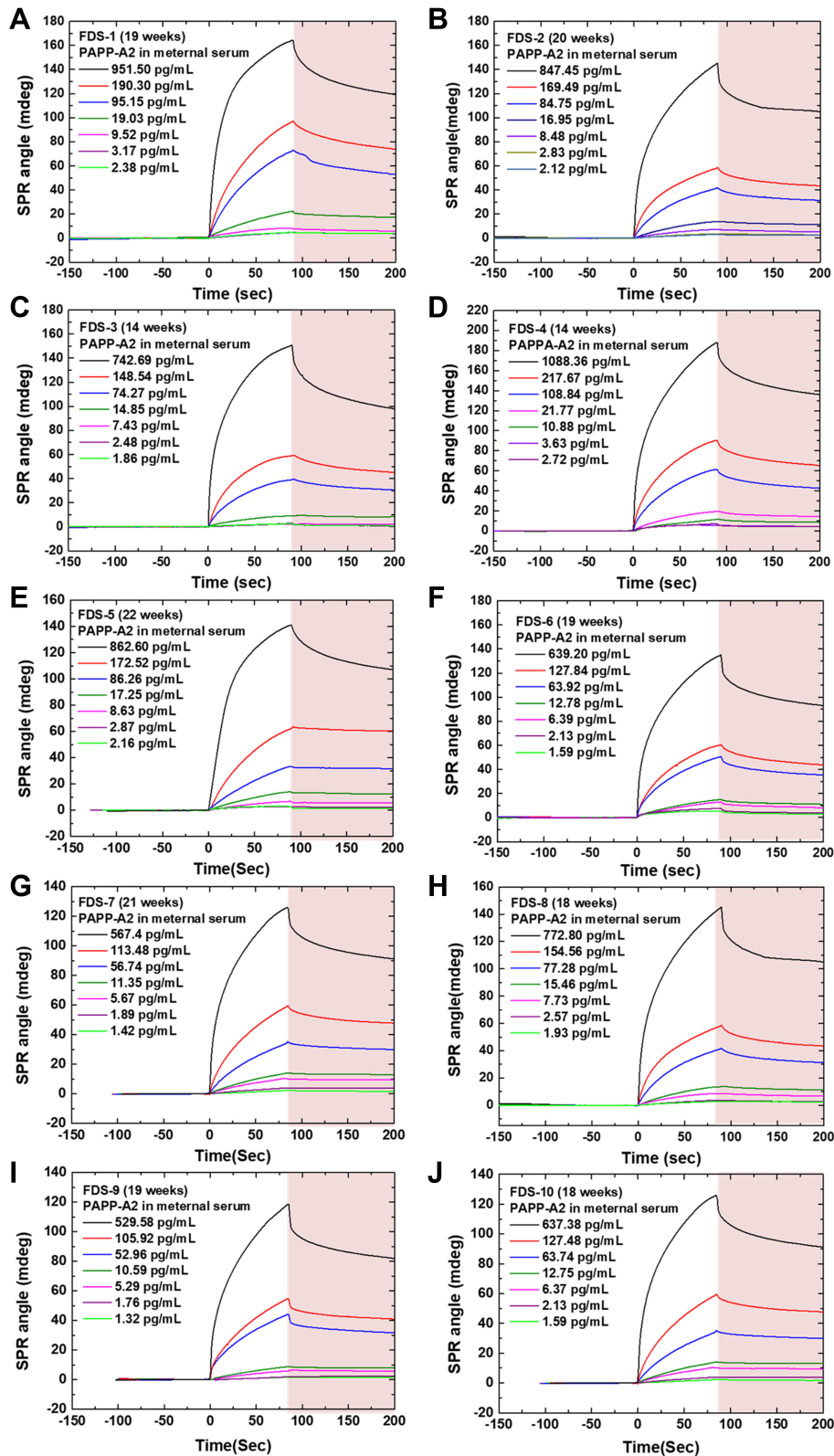


**Figure 6** Sensorgrams showing the SPR responses generated with a flow rate of 60  $\mu$ L/min and different dilution factors of 10 FDS maternal serum samples. The 10 FDS samples were derived from blood drawn at a gestational age of (A) 19, (B) 20, (C) 14, (D) 14, (E) 22, (F) 19, (G) 21, (H) 18, (I) 19, and (J) 18 weeks, respectively. **Abbreviations:** SPR, surface plasmon resonance; FDS, fetal Down's syndrome.

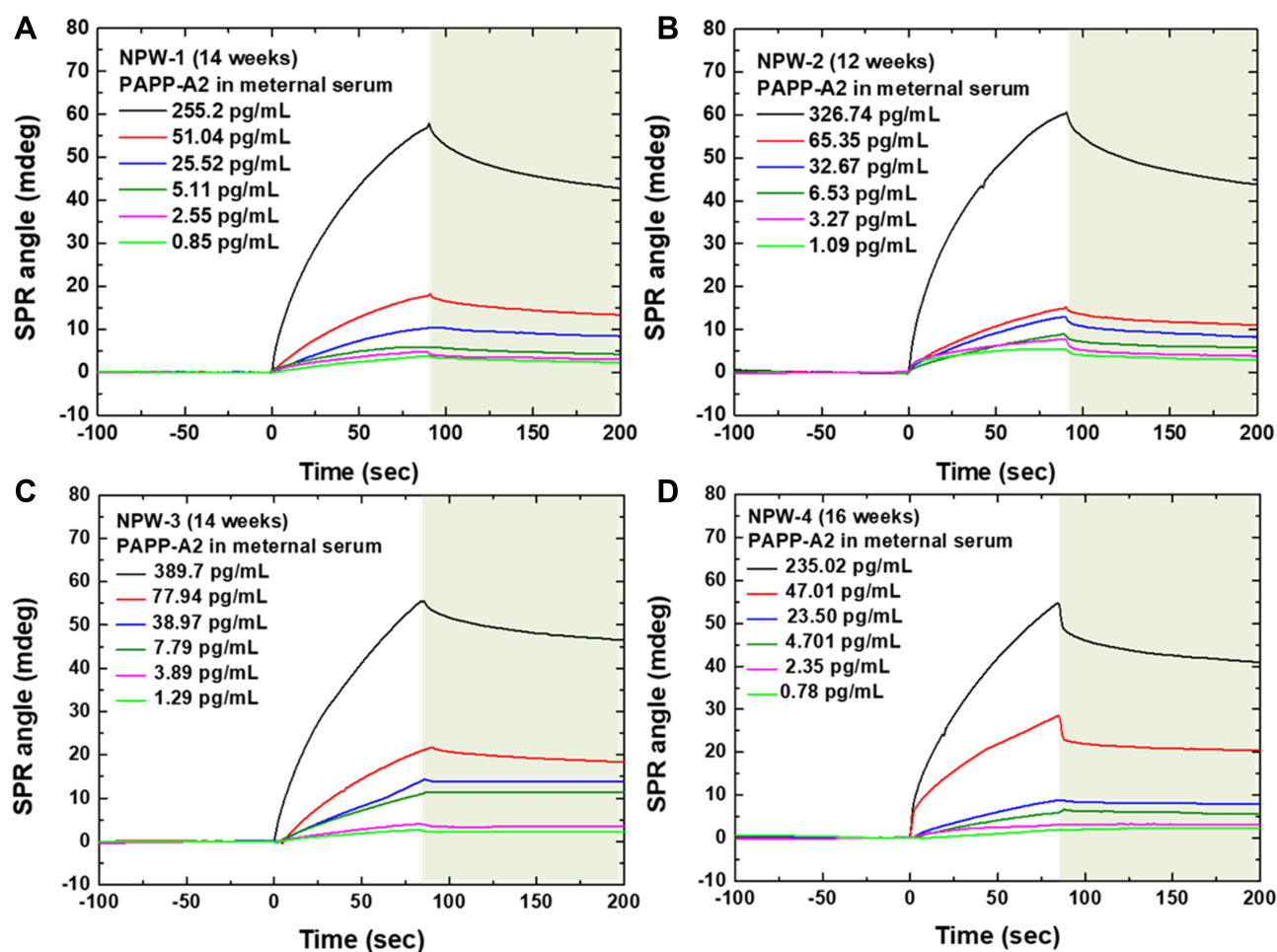


**Figure 7** Sensorgrams showing the SPR responses generated with a flow rate of  $60 \mu\text{L}/\text{min}$  and different dilution factors of maternal serum samples from four healthy women (NPW group). The NPW samples were derived from blood drawn at a gestational age of (A) 14, (B) 12, (C) 14, and (D) 16 weeks, respectively.

**Abbreviations:** SPR, surface plasmon resonance; NPW, normal pregnant women.

from 2.5 to 108 ng/mL. The regression equation of the ELISA assay was  $y = 0.03x + 0.04$  and  $R^2 = 0.97$ . The ELISA assay showed good linearity of the concentration response relationship curve signal, where  $x$  is the analyte concentration in serum, and  $y$  is the optical density (OD 450 nm).

An SPR calibration curve plotted to determine the LOD of the assay is presented in Figure 8B. The curve showed goodness of fit between the SPR angle responses obtained upon interactions of different concentrations of PAPP-A2 protein with specific anti-PAPP-A2 immobilized on the carboxyl-MoS<sub>2</sub> chip surface. The SPR responses obtained for different concentrations of PAPP-A2 protein followed a linear trend ranging from 0.1 to 1100 pg/mL. The concentration linear range had a regression equation of  $y = 0.11x + 8.54$  and a  $R^2 = 0.97$ , where  $x$  is the analyte concentration, and  $y$  is the SPR angle shift ( $m^\circ$ ). The LOD

of the SPR assay calculated on three standard deviations (SD) of the PBS buffer was 0.05 pg/mL. Error bars were calculated for four independent measurements for each concentration at a 92% confidence level.

We used two methods (SPR and ELISA) to analyze the linear correlations between the PAPP-A2 concentration in the serum of the FDS and NPW groups (Figure 8C and D). We used different dilutions (100- to 30k-fold) to compare the detected PAPP-A2 concentration within the linear curve of the response values. The experiments showed that the average PAPP-A2 concentration in the NPW group was 30.16 ng/mL (25.52, 32.67, 38.97 and 23.50 ng/mL). Under different clinical serum sample experimental conditions, the angle shift of the SPR signal ranged from 2.07 to 46.57  $m^\circ$ , and the PAPP-A2 concentration ranged from 0.78 to 389 pg/mL (100- to 30k-fold dilution) as shown in Figure 8C. In addition, the serum samples of

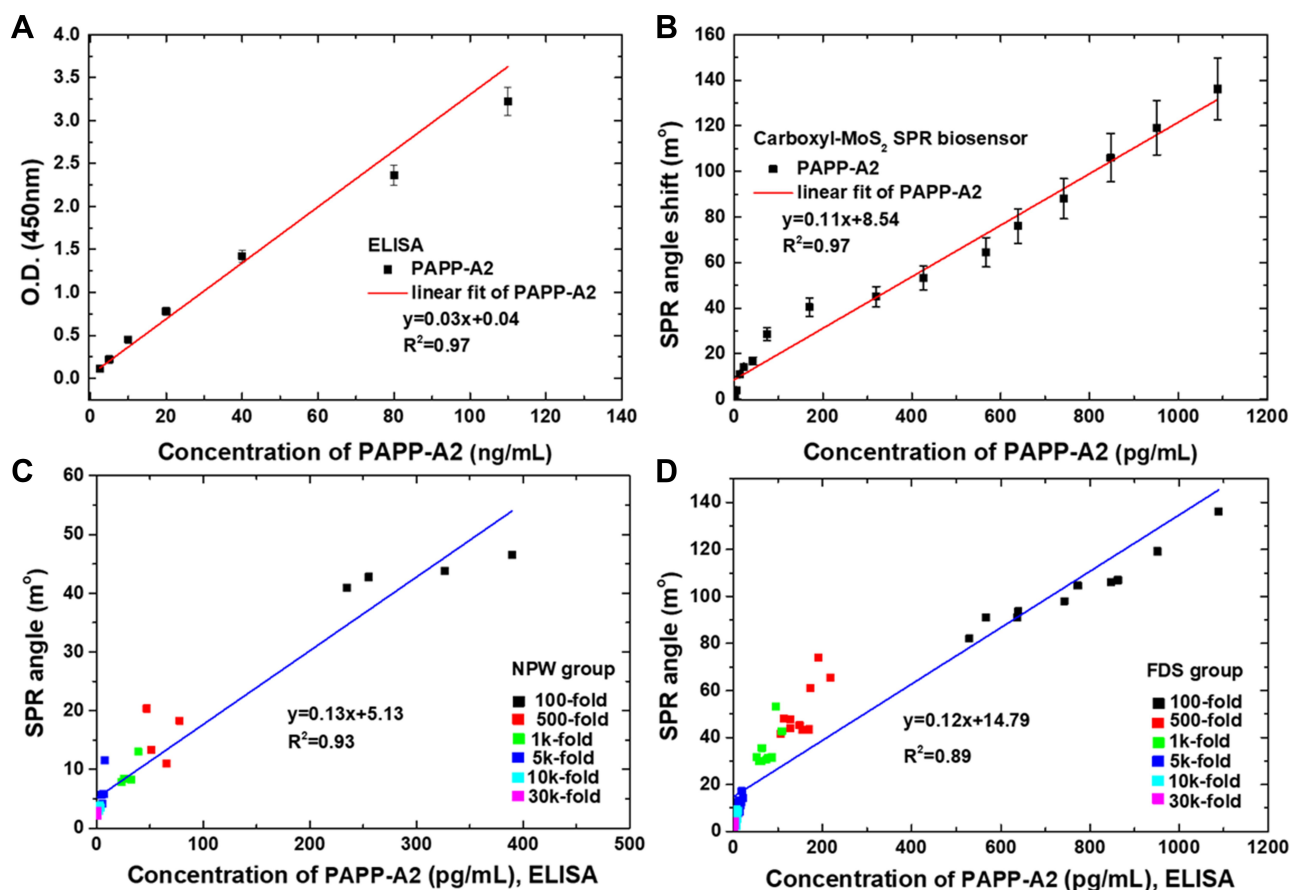


**Figure 8** Calibration curves obtained with (A) ELISA kit assays for PAPP-A2 quantification ranging from 0.1 to 108 ng/mL. (B) Calibration curve of the average SPR response to various PAPP-A2 concentrations ranging from 0.1 to 1100 pg/mL with the carboxyl-MoS<sub>2</sub>-based SPR chip. Error bars indicate standard deviations of means obtained from three replicates using SPR and three replicates using ELISA. Correlation between the concentration of PAPP-A2 in serum obtained by ELISA and signal responses by SPR. (C) NPW group (n = 24, R<sup>2</sup> = 0.97) and (D) FDS group (n = 60, R<sup>2</sup> = 0.91) samples.

**Abbreviations:** ELISA, enzyme-linked immunosorbent assay; PAPP-A2, pregnancy-associated plasma protein-A2; SPR, surface plasmon resonance; carboxyl-MoS<sub>2</sub>, carboxyl-molybdenum disulfide; NPW, normal pregnant women; FDS, fetal Down's syndrome.

the FDS group had a higher average PAPP-A2 concentration of 76.39 ng/mL (95.15, 84.75, 74.27, 108.84, 86.26, 63.92, 56.74, 77.28, 52.96, and 63.74 ng/mL), so we diluted these samples by 100- to 30k-fold for PAPP-A2 concentrations ranging from 1.32 to 1088.36 pg/mL, resulting in an SPR signal shift from 1.18 to 136.14 m° as shown in Figure 8D.

The results showed that the concentration linear range had a regression equation of  $y = 0.13x + 5.13$  and a  $R^2 = 0.93$  for the NPW group (Figure 8C) and  $y = 0.12x + 14.79$  and a  $R^2 = 0.89$  for the FDS group (Figure 8D), where  $x$  is the analyte concentration, and  $y$  is the SPR angle shift (m°). These results indicated that the SPR biosensor had higher sensitivity than the commercial ELISA kit in quantifying PAPP-A2 in the samples.

To further validate the successful fabrication of the carboxyl-MoS<sub>2</sub>-based SPR chip, we evaluated the kinetics for PAPP-A2 in the serum samples. We used a single-cycle

kinetics approach to study the interaction kinetics between anti-PAPP-A2 immobilized on the SPR chip surface and PAPP-A2, and the binding affinities between the FDS and NPW groups. To extract the SPR kinetic parameters, the kinetic data of immune protein interactions were analyzed in the framework of the Langmuir isotherm/1:1 binding model using BI-software version 2.4.4 (Biosensing Instrument Inc., Arizona, USA). For the kinetic parameters, the calculated association rate constant ( $k_a$ ) and dissociation rate constant ( $k_d$ ) were used to determine  $K_A$  (affinity constant) of two kinetic constants through the defining relationship  $k_a/k_d$ . The smaller the equilibrium dissociation constant ( $K_D = k_d/k_a$ ), the greater the affinity of the antibody for its target. The kinetic analysis of the interactions between anti-PAPP-A2 and PAPP-A2 are summarized in Figure 9A, and the real-time SPR sensorgrams are shown in Figures 6 and 7. The  $K_D$  showed binding interactions at a 60  $\mu$ L/min flow rate in the FDS

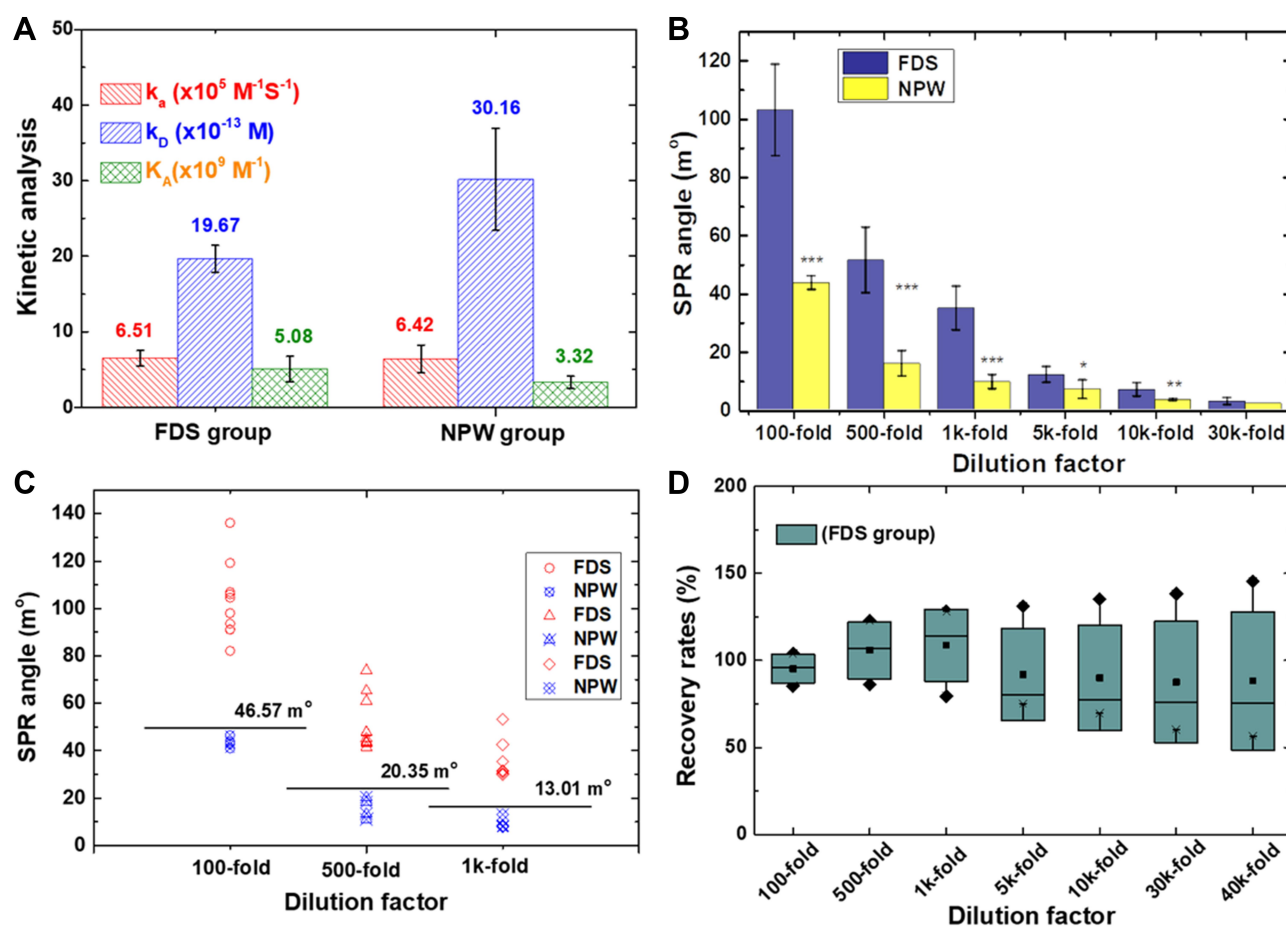


**Figure 9** SPR responses of serum samples of the FDS and NPW groups. **(A)** Kinetic analysis of the FDS and NPW groups on the carboxyl-MoS<sub>2</sub>-based SPR biosensor for affinity binding analysis of the PAPP-A2 interaction. **(B)** Correlation between two variables of the FDS and NPW groups to detect PAPP-A2 in serum samples. Data expressed as mean  $\pm$  SD for triplicate tests. Asterisks indicate statistical significance using a generalized mixed effects model (highly significant recognition (\*\*\*) ( $p < 0.001$ ); very significant recognition (\*\*\*) ( $0.001 < p < 0.01$ ); significant recognition (\*) ( $0.01 < p < 0.05$ );  $p$ : probability value). **(C)** The dot plot shows the distribution of SPR responses at the dilution rate (100-, 500-, and 1k-fold) of different serum samples and the difference between the FDS and NPW groups at the cut-off limit for screening. **(D)** Recovery rates of PAPP-A2 protein assay in the FDS group using the carboxyl-MoS<sub>2</sub>-based SPR chip.

**Abbreviations:** SPR, surface plasmon resonance; FDS, fetal Down's syndrome; NPW, normal pregnant women; carboxyl-MoS<sub>2</sub>, carboxyl-molybdenum disulfide; PAPP-A2, pregnancy-associated plasma protein-A2; SD, standard deviation.

and NPW groups, with values of  $19.67 \times 10^{-13} M$  and  $30.16 \times 10^{-13} M$ , respectively. In addition,  $k_a$  was  $6.51 \times 10^5 M^{-1}S^{-1}$  in the FDS group, which was similar to the NPW group ( $6.42 \times 10^5 M^{-1}S^{-1}$ ). The experimental results of the FDS and NPW groups showed high affinity binding to PAPP-A2 with binding constants ( $K_A$ ) of  $5.08 \times 10^9 M^{-1}$  and  $3.32 \times 10^9 M^{-1}$ , respectively.

We previously reported a carboxyl-MoS<sub>2</sub>-based SPR chip to assay BSA in PBS buffer that had a kinetic association constant  $K_A$  ( $3.9 \times 10^8 M^{-1}$ ) of 6.5-fold higher than a traditional MoS<sub>2</sub>-based SPR chip.<sup>33</sup> To assay CYFRA21-1 in spiked clinical serum samples, the dissociation constant ( $K_D$ ) ranged from  $252.6 \times 10^{-9}$  to  $980.3 \times 10^{-9} M$  with a 15-fold increase in affinity binding  $K_A$  compared to the traditional SPR chip.<sup>34</sup> However, the carboxyl-MoS<sub>2</sub>

-based SPR chip had the advantages of specific three-dimensional coordination sites that significantly improved binding affinity and sensitivity. The results showed that the carboxyl-MoS<sub>2</sub>-based SPR chip amplified the angle response and enhanced the high affinity constant ( $K_A$ ) to  $5.08 \times 10^9 M^{-1}$ . The experimental results demonstrated that the carboxyl-MoS<sub>2</sub>-based SPR biosensor had a high affinity and high specificity for detecting PAPP-A2 protein in the 14 clinical serum samples of the FDS and NPW groups.

In the analysis of FDS screening, we evaluated differences in PAPP-A2 protein concentration based on the correlation between different dilution factors of serum and SPR angle shift. Figure 9B shows that the SPR angle shift of the FDS group was greater than that of the NPW

group at different dilution factors, reflecting the FDS expression data. We used the Student's *t*-test to compare differences between the FDS and NPW groups and Pearson correlation coefficients to determine correlations between the parameters (SPSS version 18.0). The results showed a significant difference in SPR angle ( $p < 0.001$ ) between the FDS and NPW groups at 100-fold, 500-fold and 1k-fold serum dilution factors. In addition, the SPR angles in the FDS and NPW groups at high dilution factors (5k, 10k, and 30k) were significantly reduced, and there were no statistically significant differences between the two groups at 5k, 10k and 30k serum dilution factors as shown in Figure 9B.

As shown in Figure 9C, 100-, 500- and 1k-fold dilution factors of serum samples of the FDS and NPW groups were tested for the level of PAPP-A2 protein using the SPR biosensor assay to screen for FDS. To investigate the relationship between the SPR angle and different dilution factors, we analyzed the SPR angle cut-off threshold level (prevalence threshold) to screen for FDS, which was defined as an SPR angle response value greater than twice the SD above the mean response of the NPW group. In the serum with 100-fold dilution factor, the PAPP-A2 protein levels in the FDS group were increased compared to those in the NPW group, and the women with a serum PAPP-A2 concentration  $>255.20$  pg/mL had a higher correlation with FDS compared to the NPW. This result showed that the women with a cut-off SPR angle  $>46.57$  m° were more significantly associated with FDS compared to the NPW for the serum dilution factor of 100-fold. In addition, cut-off SPR angles  $>20.35$  m° (47.0 pg/mL) for 500-fold dilution and  $>13.01$  m° (38.97 pg/mL) for 1k-fold dilution were more significantly associated with FDS compared to the NPW. Moreover, the differential diagnosis in the FDS group compared to NPW group using 100-fold dilution factor was better than that of 500- and 1k-fold dilution factors. The mean SPR angle response in the FDS screening for the 100-fold dilution factor differed significantly with the NPW and FDS groups.

As shown in Figure 9D, we evaluated the recovery rate of the carboxyl-MoS<sub>2</sub>-based SPR chip and verified the reliability of PAPP-A2 detection in human serum. The recovery tests were performed using FDS group serum with different dilution factors (100- to 40k-fold) to detect PAPP-A2 protein. The serum samples were then subjected to four repeated recovery test experiments at different dilution factors.

In the FDS group, dilutions of 500-, 1k-, 5k-, 10k-, 30k-, and 40k-fold had recovery rates of 86–123%, 79–128%, 75–131%, 69–135%, 60–138%, and 56–145%, respectively. The average recovery rates of the 500-, 1k-, 5k-, 10k-, 30k-, and 40k-fold serum dilutions were 105.7%, 108.7%, 91.7%, 90.0%, 87.5% and 88.2%, with relative standard deviations (RSDs) of 8.55, 17.05, 21.08, 29.36, 31.48, 34.92 and 38.79%, respectively. In the 100-fold dilution, the recovery rates were within the range 85–104%, with an average recovery rate of 95.2% and RSD of 8.5%. These results showed the excellent binding affinity, high sensitivity, low detection limit, good stability and specificity of the carboxyl-MoS<sub>2</sub>-based SPR chip to detect PAPP-A2 protein in maternal serum to identify fetuses with FDS.

The Student's *t* test and Fisher's exact test were used to compare maternal age, time of miscarriage, and SPR angle shifts of the serum diluted 100-fold between the FDS and NPW clinical samples (Table 1). We found that maternal age was significantly higher in the FDS group ( $37.20 \pm 4.52$  years) than in the NPW group ( $30.25 \pm 2.87$  years) ( $p = 0.015$ ). No significant difference was noted in time of miscarriage between the FDS and NPW groups. In addition, significantly larger SPR angle shifts were noted in the FDS group ( $102.88 \pm 15.71$  m°) compared to the NPW group ( $43.52 \pm 2.34$  m°) ( $p < 0.001$ ).

## Conclusions

Carboxyl-MoS<sub>2</sub>-based chips are a promising new type of biosensor with the potential for high sensitivity, high affinity and label-free determination. The unique electronic and optical properties will benefit the future development of SPR-based biosensors. Importantly, PAPP-A2 protein can be used as a biomarker for effective clinical screening

**Table 1** Comparison Between the FDS and NPW Clinical Samples

	FDS	NPW	<i>p</i> value
Maternal age (years)	$37.20 \pm 4.52$	$30.25 \pm 2.87$	0.015
Miscarriage (times)			0.105
0	3 (30%)	4 (100%)	
1	3 (30%)	0 (0%)	
2	4 (40%)	0 (0%)	
SPR angle (millidegrees)	$102.88 \pm 15.71$	$43.52 \pm 2.34$	$< 0.001$

**Notes:** Continuous variables are presented as mean  $\pm$  standard deviation and categorical variables as n (%).  $p < 0.05$  was considered statistically significant.

**Abbreviations:** FDS, fetal Down's syndrome; NPW, normal pregnant women; SPR, surface plasmon resonance.



and evaluation of DS and prenatal fetal health signs. Carboxyl-MoS<sub>2</sub>-based SPR biosensors offer the benefits of simplicity and low cost of development, the probability of success for many target assays, and as a rapid and effective assay to detect DS biomarkers in serum. The objective of the present study was to establish associations between the level of PAPP-A2 in the serum of pregnant women and SPR angle to screen for DS. The experimental results showed the underlying mechanism of the association between PAPP-A2 up-regulation and DS screening. Under optimized conditions, the proposed carboxyl-MoS<sub>2</sub>-based SPR biosensor exhibited excellent analytical performance for PAPP-A2 with a wide linear range and low detection limit in the detection of clinical serum samples. The results showed that the women with a cut-off SPR angle >46.57 m° and PAPP-A2 concentration >255.20 pg/mL were more significantly associated with FDS compared to the NPW at a serum dilution factor of 100-fold. MoS<sub>2</sub> chemical functionalization is still in its infancy; however, the use of MoS<sub>2</sub> will grow quickly if it follows the covalent modification of other nanocomposites in biosensor applications. Carboxyl-MoS<sub>2</sub>-based SPR biosensors may be a new tool for clinical serum sample detection. Our experimental results successfully showed that carboxyl-MoS<sub>2</sub>-based functional materials show promise as potential sensing materials.

## Data Sharing Statement

The datasets generated for this study are available on request to the corresponding author.

## Ethics Statement

This study was conducted in accordance with the Declaration of Helsinki Ethical Principles. The authors would like to thank Mackay Memorial Hospital, Taipei, Taiwan. This work was approved by the Institutional Review Board (IRB) of Mackay Memorial Hospital for Human Clinical Trials (Permit Numbers: 15MMHIS020, 15MMHIS115 and 17MMHIS185). All experiments were performed in compliance with the relevant laws and institutional guidelines, and the Human Subjects Research Ethics Committee of Mackay Memorial Hospital approved the experiments.

## Acknowledgments

This study was supported by the Ministry of Science and Technology of the Republic of China (ROC), Taiwan, for financially supporting this research under Contract No.

MOST 105-2221-E-003-027, MOST 106-2221-E-003-020, MOST 107-2221-E-003-009, MOST 108-2221-E-003 -020 -MY3, MOST 109-2314-B-195-012-MY3, MOST 109-2221-E-003-028-MY3 also Mackay Memorial Hospital (Project No. MMH-CT-10505). We thank National Synchrotron Radiation Research Center (NSRRC, Taiwan Light Source) for their help in analyzing XPS and FTIR spectra (Beamline 09A2, 24A1 and 14A1).

## Disclosure

Prof. Dr. Nan-Fu Chiu reports a patent US10634613B2 issued, a patent US10815259B2.

The authors declare that the research was conducted in the absence of any other commercial or financial relationships that could be construed as a potential conflict of interest.

## References

1. Heffner LJ. Advanced maternal age – how old is too old? *N Engl J Med.* 2004;351:1927–1929. doi:10.1056/NEJMp048087
2. Resta RG. Changing demographics of advanced maternal age (AMA) and the impact on the predicted incidence of Down syndrome in the United States: implications for prenatal screening and genetic counseling. *Am J Med Genet A.* 2005;133A(1):31–36. doi:10.1002/ajmg.a.30553
3. Bayrampour H, Heaman M, Duncan KA, Tough S. Advanced maternal age and risk perception: a qualitative study. *BMC Pregnancy Childbirth.* 2012;12(1):100–113. doi:10.1186/1471-2393-12-100
4. Kahveci B, Melekoglu R, Evruke IC, Cetin C. The effect of advanced maternal age on perinatal outcomes in nulliparous singleton pregnancies. *BMC Pregnancy Childbirth.* 2018;18(1):343–349. doi:10.1186/s12884-018-1984-x
5. Carr J, Collins S. 50 years with Down syndrome: a longitudinal study. *J Appl Res Intellect Disabil.* 2018;31:743–750. doi:10.1111/jar.12438
6. Shin M, Besser LM, Kucik JE, Lu C, Siffel C, Correa A. Prevalence of Down syndrome among children and adolescents in 10 regions of the United States. *Pediatrics.* 2009;124(6):1565–1571. doi:10.1542/peds.2009-0745
7. Parker SE, Mai CT, Canfield MA, et al. Updated national birth prevalence estimates for selected birth defects in the United States, 2004–2006. *Birth Defects Res Part A Clin Mol Teratol.* 2010;88:1008–1016. doi:10.1002/bdra.20735
8. Feigin V. Global, regional, and national incidence, prevalence, and years lived with disability for 310 diseases and injuries, 1990–2015: a systematic analysis for the Global Burden of Disease Study 2015. *Lancet.* 2016;388:1545–1602. doi:10.1016/S0140-6736(16)31678-6
9. Wang H, Naghavi M, Allen C, et al. Global, regional, and national life expectancy, all-cause mortality, and cause-specific mortality for 249 causes of death, 1980–2015: a systematic analysis for the Global Burden of Disease Study 2015. *Lancet.* 2016;388:1459–1544. doi:10.1016/S0140-6736(16)31012-1
10. Taylor-Phillips S, Freeman K, Geppert J, et al. Accuracy of non-invasive prenatal testing using cell-free DNA for detection of Down, Edwards and Patau syndromes: a systematic review and meta-analysis. *BMJ Open.* 2016;6(1):e010002. doi:10.1136/bmjopen-2015-010002

11. Twiss P, Hill M, Daley R, et al. Non-invasive prenatal testing for Down syndrome. *Semin Fetal Neonatal Med.* 2014;19(1):9–14. doi:10.1016/j.siny.2013.10.003
12. Sillence KA, Madgett TE, Roberts LA, Overton TG, Avent ND. Non-invasive screening tools for down's syndrome: a review. *Diagnostics.* 2013;3(2):291–314. doi:10.3390/diagnostics3020291
13. Nicolaides KH. Screening for fetal aneuploidies at 11 to 13 weeks. *Prenat Diagn.* 2011;31:7–15. doi:10.1002/pd.2637
14. Wald NJ, Kennard A, Hackshaw A, McGuire A. Antenatal screening for Down's syndrome. *J Medical Screening.* 1997;4:181–246. doi:10.1177/096914139700400402
15. Cuckle HS, Holding S, Jones R, Groome NP, Wallace EM. Combining Inhibin A with existing second-trimester markers in maternal serum screening for Down's syndrome. *Prenat Diagn.* 1996;16:1095–1100. doi:10.1002/(SICI)1097-0223(199612)16:12<1095::AID-PD997>3.0.CO;2-9
16. Shaw SWS, Chen CP, Cheng PJ. From Down syndrome screening to noninvasive prenatal testing: 20 years' experience in Taiwan. *Taiwan J Obstet Gynecol.* 2013;52:470–474. doi:10.1016/j.tjog.2013.10.003
17. Munnangi S, Gross SJ, Mudankamar R, Salcedo G, Reznik SE. Pregnancy associated plasma protein-A2: a novel biomarker for down syndrome. *Placenta.* 2014;35:900–906. doi:10.1016/j.placenta.2014.08.001
18. Nishizawa H, Pryor-Koishi K, Suzuki M, Kato T, Kogo H, Sekiya T. Increased levels of pregnancy-associated plasma protein-A2 in the serum of pre-eclamptic patients. *Mol Hum Reprod.* 2008;14(10):595–602. doi:10.1093/molehr/gan054
19. Overgaard MT, Boldt HB, Laursen LS, et al. Pregnancy-associated plasma protein-A2 (PAPP-A2), a novel insulin-like growth factor-binding protein-5 proteinase. *J Biol Chem.* 2001;276(24):21849–21853. doi:10.1074/jbc.M102191200
20. Kløverpris S, Gaidamuskas E, Rasmussen LCV, et al. A robust immunoassay for pregnancy-associated plasma protein-A2 based on analysis of circulating antigen: establishment of normal ranges in pregnancy. *Mol Hum Reprod.* 2013;19(11):756–763. doi:10.1093/molehr/gat047
21. Kalousova M, Dusilova-Sulkova S, Kubena AA, et al. Pregnancy-associated plasma protein A2 in hemodialysis patients: significance for prognosis. *Kidney Blood Press Res.* 2017;42(3):509–518. doi:10.1159/000479847
22. Bockova M, Chadtova Song X, Gedeonova E, et al. Surface plasmon resonance biosensor for detection of pregnancy associated plasma protein A2 in clinical samples. *Anal Bioanal Chem.* 2016;408(26):7265–7269. doi:10.1007/s00216-016-9664-z
23. Chiu NF, Tai MJ, Wu HP, Lin TL, Chen CY. Development of a bioaffinity SPR immunosensor based on functionalized graphene oxide for the detection of pregnancy-associated plasma protein A2 in human plasma. *Int J Nanomedicine.* 2019;14:6735–6748. doi:10.2147/IJN.S213653
24. Fan SY, Chiu NF, Chen CP, Chang CC, Chen CY. Simultaneous real-time detection of pregnancy-associated plasma protein-A and-A2 using a graphene oxide-based surface plasmon resonance biosensor. *Int J Nanomedicine.* 2020;15:2085–2094. doi:10.2147/IJN.S237938
25. Chiu NF, Kuo CT, Chen CY. High-affinity carboxyl-graphene oxide-based SPR aptasensor for the detection of hCG protein in clinical serum samples. *Int J Nanomed.* 2019;14:4833–4847. doi:10.2147/IJN.S208292
26. Chiu NF, Wang YH, Chen CY. Clinical application for screening Down's Syndrome by using carboxylated graphene oxide-based surface plasmon resonance aptasensors. *Int J Nanomedicine.* 2020;15:8131–8149. doi:10.2147/IJN.S270938
27. Soni A, Pandey CM, Pandey MK, Sumana G. Highly efficient Polyaniline-MoS<sub>2</sub> hybrid nanostructures based biosensor for cancer biomarker detection. *Anal Chim Acta.* 2019;1055:26–35. doi:10.1016/j.aca.2018.12.033
28. Chu Y, Cai B, Ma Y, Zhao M, Ye Z, Huang J. Highly sensitive electrochemical detection of circulating tumor DNA based on thin-layer MoS<sub>2</sub>/graphene composites. *RSC Adv.* 2016;6:22673–22678. doi:10.1039/C5RA27625J
29. Cai B, Guo S, Li Y. MoS<sub>2</sub>-based sensor for the detection of miRNA in serum samples related to breast cancer. *Anal Methods.* 2018;10:230–236. doi:10.1039/C7AY02329D
30. Lee J, Dak P, Lee Y, et al. Two-dimensional layered MoS<sub>2</sub> biosensors enable highly sensitive detection of biomolecules. *Sci Rep.* 2014;4:1–7. doi:10.1038/srep07352
31. Liu J, Chen X, Wang Q, et al. Ultrasensitive monolayer MoS<sub>2</sub> field-effect transistor based DNA sensors for screening of Down Syndrome. *Nano Lett.* 2019;19:1437–1444. doi:10.1021/acs.nanolett.8b03818
32. Rahman MS, Anower MS, Rahman MK, et al. Modeling of a highly sensitive MoS<sub>2</sub>-Graphene hybrid based fiber optic SPR biosensor for sensing DNA hybridization. *Optik.* 2017;140:989–997. doi:10.1016/j.rinp.2019.102623
33. Chiu NF, Lin TL. Affinity capture surface carboxyl-functionalized MoS<sub>2</sub> sheets to enhance the sensitivity of surface plasmon resonance immunosensors. *Talanta.* 2018;185:174–181. doi:10.1016/j.talanta.2018.03.073
34. Chiu NF, Yang HT. High-sensitivity detection of the lung cancer biomarker CYFRA21-1 in serum samples using a carboxyl-MoS<sub>2</sub> functional film for SPR-based immunosensors. *Front Bioeng Biotechnol.* 2020;8:1–14. doi:10.3389/fbioe.2020.00234
35. Nurrohman DT, Wang YH, Chiu NF. Exploring graphene and MoS<sub>2</sub> chips based surface plasmon resonance biosensors for diagnostic applications. *Front Chem.* 2020;8:1–17. doi:10.3389/fchem.2020.00728
36. Singhal C, Khanuja M, Chaudhary N, Pundir CS, Narang J. Detection of chikungunya virus DNA using two-dimensional MoS<sub>2</sub> nanosheets based disposable biosensor. *Sci Rep.* 2018;8(1):1–11. doi:10.1038/s41598-018-25824-8
37. Li J, Zhang W, Lei H, Li B. MoS<sub>2</sub>-based nanocomposites for surface enhanced Raman scattering. *Proc SPIE.* 2017;10622:1–9. doi:10.1117/12.2288614
38. Kolluru GK, Shen X, Bir SC, Kevil CG. Hydrogen sulfide chemical biology: pathophysiological roles and detection. *Nitric Oxide.* 2013;35:5–20. doi:10.1016/j.niox.2013.07.002
39. Steiger AK, Zhao Y, Pluth MD. Emerging roles of carbonyl sulfide in chemical biology: sulfide transporter or gasotransmitter? *Antioxidants Redox Signaling.* 2018;28:1516–1532. doi:10.1089/ars.2017.7119
40. Sarkar D, Liu W, Xie X, et al. MoS<sub>2</sub> field-effect transistor for next-generation label-free biosensors. *ACS Nano.* 2014;8:3992–4003. doi:10.1021/nn5009148
41. Majee BP, Srivastava V, Mishra AK. Surface-enhanced Raman scattering detection based on an interconnected network of vertically oriented semiconducting few-layer MoS<sub>2</sub> nanosheets. *ACS Appl Nano Mater.* 2020;3:4851–4858. doi:10.1021/acsanm.0c00979
42. Zeng S, Hu S, Xia J, et al. Graphene-MoS<sub>2</sub> hybrid nanostructures enhanced surface plasmon resonance biosensors. *Sens Actuators B.* 2015;207:801–810. doi:10.1016/j.snb.2014.10.124
43. Maurya JB, Prajapati YK, Tripathi R. Effect of molybdenum disulfide layer on surface plasmon resonance biosensor for the detection of bacteria. *Silicon.* 2018;10(2):245–256. doi:10.1007/s12633-016-9431-y
44. Presolski S, Pumera M. Covalent functionalization of MoS<sub>2</sub>. *Materials Today.* 2016;19(3):140–145. doi:10.1016/j.mattod.2015.08.019
45. Yang L, Majumdar K, Liu H, et al. Chloride molecular doping technique on 2D materials: WS<sub>2</sub> and MoS<sub>2</sub>. *Nano Lett.* 2014;14:6275–6280. doi:10.1021/nl502603d
46. Chiu NF, Lin TL. Method of synthesizing carboxyl-modified molybdenum disulfide. US10815259B2; 2018.

47. Chiu NF, Lin TL. Molybdenum disulfide-containing biosensing chip and detection device comprising the biosensing chip. *US2019 0219504A1*; 2018.
48. Yang X, Meng N, Zhu Y, Zhou Y, Nie W, Chen P. Greatly improved mechanical and thermal properties of chitosan by carboxyl-functionalized MoS<sub>2</sub> nanosheets. *J Mater Sci*. 2016;51(3):1344–1353. doi:10.1007/s10853-015-9453-7
49. Chiu NF, Fan SY, Yang CD, Huang TY. Carboxyl-functionalized graphene oxide composites as SPR biosensors with enhanced sensitivity for immunoaffinity detection. *Biosens Bioelectron*. 2017;89:370–376. doi:10.1016/j.bios.2016.06.073
50. Yin X, Wang Q, Cao L, et al. Tunable inverted gap in monolayer quasi-metallic MoS<sub>2</sub> induced by strong charge-lattice coupling. *Nat Comm*. 2017;8(1):1–9. doi:10.1038/s41467-017-00640-2
51. Addou R, McDonnell S, Barrera D, et al. Impurities and electronic property variations of natural MoS<sub>2</sub> crystal surfaces. *ACS Nano*. 2015;9:9124–9133. doi:10.1021/acs.nano.5b03309
52. Jung C, Yang HI, Choi W. Effect of ultraviolet-ozone treatment on MoS<sub>2</sub> monolayers: comparison of chemical-vapor-deposited polycrystalline thin films and mechanically exfoliated single crystal flakes. *Nanoscale Res Lett*. 2019;14(1):1–8. doi:10.1186/s11671-019-3119-3
53. Tsai M, Su SH, Chang JK, et al. Monolayer MoS<sub>2</sub> heterojunction solar cells. *ACS Nano*. 2014;8:8317–8322. doi:10.1021/NN502776H
54. Fang Y, Lv Y, Gong F, et al. Synthesis of 2D-mesoporous-carbon/MoS<sub>2</sub> heterostructures with well-defined interfaces for high-performance lithium-ion batteries. *Adv Mater*. 2016;28:9385–9390. doi:10.1002/adma.201602210
55. Chou SS, De M, Kim J, et al. Ligand conjugation of chemically exfoliated MoS<sub>2</sub>. *J Am Chem Soc*. 2013;135:4584–4587. doi:10.1021/ja310929s
56. Li DB, Sun XJ, Jia YP, et al. Direct observation of localized surface plasmon field enhancement by Kelvin probe force microscopy. *Light*. 2017;6:17038. doi:10.1038/lsa.2017.38
57. Furube A, Hashimoto S. Insight into plasmonic hot-electron transfer and plasmon molecular drive: new dimensions in energy conversion and nanofabrication. *NPG Asia Materials*. 2017;9(12):1–24. doi:10.1038/am.2017.191
58. Zhang J, Wang P, Sun J. High-efficiency plasmon-enhanced and graphene-supported semiconductor/metal core-satellite heteronano-crystal photocatalysts for visible-light dye photodegradation and H<sub>2</sub> production from water. *ACS Appl Mater Interfaces*. 2014;6:19905–19913. doi:10.1021/am505371g
59. Wang Y, Ou JZ, Chrimes AF, et al. Plasmon resonances of highly doped two-dimensional MoS<sub>2</sub>. *Nano Lett*. 2015;15:883–890. doi:10.1021/nl503563g
60. Chiu NF, Huang TY. Sensitivity and kinetic analysis of graphene oxide-based surface plasmon resonance biosensors. *Sens Actuators B Chem*. 2014;197:35–42. doi:10.1016/j.snb.2014.02.033
61. Chiu NF, Kuo CT, Lin TL, et al. Ultra-high sensitivity of the non-immunological affinity of graphene oxide-peptide-based surface plasmon resonance biosensors to detect human chorionic gonadotropin. *Biosens Bioelectron*. 2017;94:351–357. doi:10.1016/j.bios.2017.03.008
62. Chiu NF, Lin TL, Kuo CT. Highly sensitive carboxyl-graphene oxide-based surface plasmon resonance immunosensor for the detection of lung cancer for cytokeratin 19 biomarker in human plasma. *Sens Actuators B Chem*. 2018;265:264–272. doi:10.1016/j.snb.2018.03.070

International Journal of Nanomedicine

Dovepress

Publish your work in this journal

The International Journal of Nanomedicine is an international, peer-reviewed journal focusing on the application of nanotechnology in diagnostics, therapeutics, and drug delivery systems throughout the biomedical field. This journal is indexed on PubMed Central, MedLine, CAS, SciSearch®, Current Contents®/Clinical Medicine,

Journal Citation Reports/Science Edition, EMBase, Scopus and the Elsevier Bibliographic databases. The manuscript management system is completely online and includes a very quick and fair peer-review system, which is all easy to use. Visit <http://www.dovepress.com/testimonials.php> to read real quotes from published authors.

Submit your manuscript here: <https://www.dovepress.com/international-journal-of-nanomedicine-journal>